Mutant *KRAS* Mediates circARFGEF2 Biogenesis to Promote Lymphatic Metastasis of Pancreatic Ductal Adenocarcinoma

Yao Kong[1,2], Yuming Luo[1], Shangyou Zheng[1], Jiabin Yang[1,3], Dingwen Zhang[1,3], Yue Zhao[4], Hanhao Zheng[5,6], Mingjie An[5,6], Yan Lin[5,6], Le Ai[6,7], Xiayao Diao[8], Qing Lin[1], Changhao Chen[5,6], and Rufu Chen[1,3,9]

ABSTRACT

Circular RNAs (circRNA) contribute to cancer stemness, proliferation, and metastasis. The biogenesis of circRNAs can be impacted by the genetic landscape of tumors. Herein, we identified a novel circRNA, circARFGEF2 (hsa_circ_0060665), which was upregulated in $KRAS^{G12D}$ pancreatic ductal adenocarcinoma (PDAC) and positively associated with $KRAS^{G12D}$ PDAC lymph node (LN) metastasis. CircARFGEF2 overexpression significantly facilitated $KRAS^{G12D}$ PDAC LN metastasis *in vitro* and *in vivo*. Mechanistically, circARFGEF2 biogenesis in $KRAS^{G12D}$ PDAC was significantly activated by the alternative splicing factor QKI-5, which recruited U2AF35 to facilitate spliceosome assembly. QKI-5 bound the QKI binding motifs and neighboring reverse complement sequence in intron 3 and 6 of *ARFGEF2* pre-mRNA to facilitate circARFGEF2 biogenesis. CircARFGEF2 sponged miR-1205 and promoted the activation of JAK2, which phosphorylated STAT3 to trigger $KRAS^{G12D}$ PDAC lymphangiogenesis and LN metastasis. Importantly, circARFGEF2 silencing significantly inhibited LN metastasis in the $Kras^{G12D/+}Trp53^{R172H/+}$Pdx-1-Cre (KPC) mouse PDAC model. These findings provide insight into the mechanism and metastasis-promoting function of mutant KRAS-mediated circRNA biogenesis.

Significance: Increased splicing-mediated biogenesis of circARFGEF2 in *KRAS*-mutant pancreatic ductal adenocarcinoma activates JAK2–STAT3 signaling and triggers lymph node metastasis, suggesting circARFGEF2 could be a therapeutic target to inhibit pancreatic cancer progression.

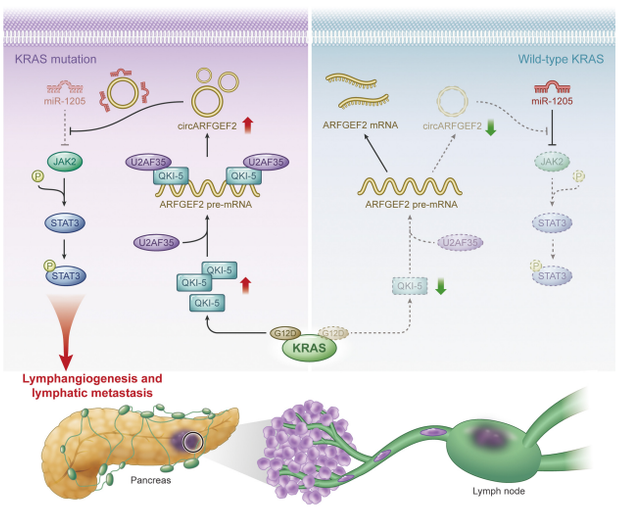

Introduction

Pancreatic ductal adenocarcinoma (PDAC) is one of the deadliest digestive system malignancies; its incidence is increasing and it is predicted to be the second most common cause of death within the next decade (1, 2). *KRAS* mutations were identified in approximately 90% of patients with PDAC and $KRAS^{G12D}$ was the most common allele in PDAC (3, 4). Gene therapy targeting the $KRAS^{G12D}$ mutation achieved 70% regression in metastatic PDAC, indicating the therapeutic potential of $KRAS^{G12D}$ in metastatic PDAC (5). Lymph node (LN) metastasis is an important metastatic route in PDAC. Recent studies demonstrated the increased tendency of LN metastasis in

[1]Department of Pancreas Center, Department of General Surgery, Guangdong Provincial People's Hospital (Guangdong Academy of Medical Sciences), Southern Medical University, Guangzhou, Guangdong, P.R. China. [2]Guangdong Cardiovascular Institute, Guangdong Provincial People's Hospital, Guangdong Academy of Medical Sciences, Guangzhou, Guangdong, P.R. China. [3]School of Medicine, South China University of Technology, Guangzhou, Guangdong, P.R. China. [4]Department of Tumor Intervention, Sun Yat-sen University First Affiliated Hospital, Guangzhou, Guangdong, P.R. China. [5]Department of Urology, Sun Yat-sen Memorial Hospital, Sun Yat-sen University, Guangzhou, Guangdong, P.R. China. [6]Guangdong Provincial Key Laboratory of Malignant Tumor Epigenetics and Gene Regulation, Sun Yat-sen Memorial Hospital, State Key Laboratory of Oncology in South China, Guangzhou, Guangdong, P.R. China. [7]Department of Oncology, Sun Yat-sen Memorial Hospital, Sun Yat-sen University, Guangzhou, Guangdong, P.R. China. [8]Department of Thoracic Surgery, Peking Union Medical College Hospital, Chinese Academy of Medical Sciences and Peking Union Medical College, Beijing, P.R. China. [9]The Second School of Clinical Medicine, Southern Medical University, Guangzhou, Guangdong, P.R. China.

Y. Kong, Y. Luo, S. Zheng, and J. Yang contributed equally to this article.

Corresponding Authors: Rufu Chen, Department of General Surgery, Guangdong Provincial People's Hospital, Guangzhou, 510120, China. E-mail: chenrf63@163.com; and Changhao Chen, Department of Urology, Sun Yat-sen Memorial Hospital, 107 Yanjiangxi Road, Yuexiu District, Guangzhou, Guangdong, 510120, P. R. China. E-mail: chenchh53@mail.sysu.edu.cn

Cancer Res 2023;83:3077–94

doi: 10.1158/0008-5472.CAN-22-3997

KRAS^{G12D} PDAC (6). Therefore, investigating the underlying mechanism between *KRAS*^{G12D} mutation and LN metastasis in PDAC is of great importance.

Circular RNAs (circRNA) are covalently enclosed, single-stranded RNAs that have emerged as an important class of molecule in tumorigenesis by regulating various biological processes, such as gene expression, protein translation, and binding with RNA-binding proteins (RBP; refs. 7, 8). Recently, a series of studies revealed that circRNAs are significant in *KRAS* mutant-driven cancers (9). In dividing cells, circRNAs increased the expression level of *KRAS*, which prevented senescence and enabled a proliferative phenotype of these cells (10). In bladder cancer, circRNAs activated *KRAS* signaling and decreased the chemosensitivity of bladder cancer cells to cisplatin, promoting bladder cancer invasion (11). Nevertheless, little is known about the relationship between circRNAs and *KRAS*^{G12D} mutant-driven LN metastasis in PDAC.

The traditional circRNA research paradigm mainly focused on the downstream targets of circRNAs, such as acting as endogenous competitive RNAs that sponge miRNAs and blocking the inhibitory effect of miRNAs on their target mRNAs (12). However, differing from the traditional research paradigm, recent studies provided great insight into circRNA biogenesis (13, 14). Generally, circRNA biogenesis is mediated by back-splicing of the proximity of a downstream splice site that interacts with an upstream splice site (15, 16). Recent studies demonstrated that *KRAS* mutant cells have significant circRNA expression profiles compared with other cells and the mechanism underlying back-splicing cannot fully explain why these circRNAs are abundant in *KRAS* mutant cells (9, 17). Therefore, understanding the circRNA biogenesis mechanism in *KRAS*^{G12D} PDAC is of great significance for *KRAS*^{G12D} PDAC LN metastasis.

Quaking (QKI) is a member of the signal transduction and activator of RNA (STAR) family, which belongs to the hnRNPK homology (KH)-type family and is a well-known regulator of pre-mRNA alternative splicing, mRNA turnover, and translation (18, 19). Recently, QKI was identified as the culprit protein in the biogenesis of certain circRNAs by regulating pre-mRNA alternative splicing, and the majority of QKI binds within introns were revealed via specific motifs (20–22). Nonetheless, the alternative splicing mechanism is a complex process that requires the cooperation of a series of proteins, except for QKI (23). The proteins associated with QKI in regulating circRNA biogenesis remain unclear and require further investigation.

In this study, we identified a novel circRNA, circARFGEF2 (hsa_circ_0060665), which was upregulated in *KRAS*^{G12D} PDAC and positively associated with *KRAS*^{G12D} PDAC LN metastasis. Overexpressing circARFGEF2 significantly facilitated *KRAS*^{G12D} PDAC LN metastasis *in vitro* and *in vivo*. Mechanistically, circARFGEF2 biogenesis was activated by the alternative splicing factor, QKI-5, which recruited U2AF35 to facilitate spliceosome assembly and bind with the QKI binding motifs and neighboring reverse complement sequence in intron 3 and 6 of *ARFGEF2* pre-mRNA to induce circARFGEF2 biogenesis. QKI-5-mediated circARFGEF2 sponged miR-1205 and promoted the activation of JAK2, which phosphorylated STAT3 and activated the JAK2–STAT3 signaling pathway to trigger *KRAS*^{G12D} PDAC lymphangiogenesis and LN metastasis. Our findings reveal the underlying mechanism of *KRAS*^{G12D} mutation-related circRNA biogenesis and demonstrate the crucial role of circARFGEF2 in *KRAS*^{G12D} PDAC LN metastasis, indicating that circARFGEF2 might be a potential target for treating LN metastatic *KRAS*^{G12D} PDAC.

Materials and Methods

Patients and clinical samples

A total of 395 patients with PDAC who had undergone surgery and 98 patients with PDAC who had undergone biopsy at Guangdong Provincial People's Hospital, Sun Yat-sen Memorial Hospital, Sun Yat-sen University, and The Sixth Affiliated Hospital of Sun Yat-sen University were included. Fifty-two patients with lung adenocarcinoma and 57 patients with colon cancer who had undergone surgery in Sun Yat-sen Memorial Hospital, Sun Yat-sen University were included. The diagnosis of all the patients were confirmed by two professional pathologists independently. Patients with other pathological diagnosis were excluded. All samples were quickly placed in liquid nitrogen and transferred to −80°C for long-term preservation.

Cell culture

Human lymphatic endothelial cells (HLEC) were purchased from ScienCell Research Laboratories. The other cell lines were purchased from ATCC. The PANC-1 (ATCC, CRL-1469MET; RRID: CVCL_A4BT), Capan-2 (ATCC, HTB-80; RRID: CVCL_0026), and hTERT-HPNE (ATCC, CRL-4023TM; RRID: CVCL_C466) cells were cultured in DMEM (Gibco). AsPC-1 (ATCC, CRL-1682; RRID: CVCL_0152) and BxPC-3 (ATCC, CRL-1687; RRID: CVCL_0186) cells were cultured in RPMI1640 medium (Gibco). All the culture media are complete media with 10% FBS (HyClone). The HLECs were cultured with endothelial cell medium (ECM; ScienCell Research Laboratories) with 5% FBS. All cell lines were authenticated by short tandem repeat analysis and were cultured in a humid atmosphere containing 5% CO_2 at 37°C.

Determination of the physical interaction between QKI-5 and *ARFGEF2* pre-mRNA

RNA immunoprecipitation (RIP) assay was conducted according to the instructions of EZ-Magna RIP Kit (Merck, catalog no. 17-701) to identify the interaction between QKI and *ARFGEF2* pre-mRNA. Cells were incubated on ice for 5 minutes with 100 μL RIP lysis buffer, then stored at −80°C for 5 hours. Magnetic beads (50 μL) were mixed with 5 μL anti-QKI-5 antibody (Thermo Fisher, A300–183A, RRID: AB_2173160) and rotated for 30 minutes at room temperature. Then the mixture was placed in a magnetic rack to discard the supernatant and resuspended with 900 μL RIP buffer. The RIP lysis products were thawed, added to RIP buffer containing magnetic beads and antibody complex, and incubated overnight at 4°C. The centrifuge tube was placed on the magnetic rack, the supernatant discarded, the beads washed with 500 μL RIP washing buffer six times, and the RNA bound on the magnetic beads was extracted and stored on ice for further experiments.

Fluorescent assessment of lymphangiogenesis

The fluorescence assay was conducted according to the instruction of Multiple Fluorescent Immunohistochemical Kit (Panovue). Paraffin tissue sections were placed at 60°C for 2 hours, then dewaxed with xylene and hydrated with decreasing concentrations of ethanol. After washing with PBS (Biological Industries), the sections were immersed in 10% neutral formaldehyde for 10 minutes. Then the sections were placed in ethylene diamine tetraacetic acid (EDTA) buffer solution for antigen repair, then heated for 7 minutes at medium-high temperature and 14 minutes at medium-low temperature. After cooling to room temperature, the slices were blocked with catalase inhibitor for 10 minutes, washed three times with Tris Buffered Saline with Tween-20 (TBST), and sealed with goat serum. Then, the sections were

incubated with the primary antibody solution at room temperature for 1 hour and followed by HRP-labeled secondary antibody solution at room temperature for 30 minutes. Subsequently, the sections were incubated with dye working solution under dark conditions. Finally, the samples were stained with 4′,6-diamidino-2-phenylindole (DAPI) for 15 minutes. Images were captured by confocal fluorescence microscopy (Carl Zeiss AG).

Administration of WP1066 in mouse models

WP1066 was purchased from MedChemExpress (catalog no. HY-15312) and administered to the mice intraperitoneally with a dose of 40 mg/kg from Monday to Friday for 6 weeks (24, 25). The toxicity of WP1066 was dose-dependent, when exceeding 50 mg/kg per day causing diarrhea and a high frequency of urination and we did not observe any toxicities of WP1066 in this study (26).

Statistical analysis

All quantitative data were calculated as the mean ± SD of at least three independent experiments. Cumulative survival time was evaluated with Kaplan–Meier analysis and tested by the log-rank method. Independent prognostic factors were determined with multivariate Cox proportional hazards models. The relationship between unpaired variables was evaluated using the chi-square test. The relationship between paired variables was evaluated using the two-tailed Student *t* test and one-way ANOVA. $P < 0.05$ was considered statistically significant. All statistical tests were performed with SPSS (Version 19.0; IBM Corp.).

Study approval

The clinical data and specimens were obtained from patients with written informed consent. A total of 342 cases of these specimens have received the approval of the Committees for Ethical Review of Research involving Human Subjects at Sun Yat-sen Memorial Hospital [approval no. 2016 (136)]. A total of 158 cases of these specimens have received the approval of the Committees for Ethical Review of Research involving Human Subjects at Guangdong Provincial People's Hospital (approval no. KY2020–348–01). A total of 102 cases of these specimens have received the approval of the Committees for Ethical Review of Research involving Human Subjects at The Sixth Affiliated Hospital of Sun Yat-sen University (approval no. 2022ZSLYEC-295). The animal study was performed after receiving approval from the Guangdong Provincial People's Hospital (approval no. KY2020-348-01).

Data availability

RNA sequencing data generated in the study are available in Gene Expression Omnibus under accession numbers GSE234760 (https://www.ncbi.nlm.nih.gov/geo/query/acc.cgi?acc=GSE234760) and GSE234927 (https://www.ncbi.nlm.nih.gov/geo/query/acc.cgi?acc=GSE234927). More detailed methods are available in the Supplementary Materials and Methods. The data generated in this study are available within the article and Supplementary data files, as well as upon request from the corresponding author.

Results

Identification of circARFGEF2 in LN metastatic KRAS^{G12D} PDAC

To investigate whether circRNAs participate in *KRAS*^{G12D}-driven LN metastasis, we conducted next-generation sequencing in three paired PDAC tissues and normal adjacent tissues (NAT; GSE234760) and found 50 circRNAs upregulated, 58 circRNAs downregulated by >10-fold in the PDAC tissues (Supplementary Fig. S1A). Then the elevated circRNAs were evaluated in a larger cohort of 395-case patients with PDAC, which revealed that 11 circRNAs were upregulated in PDAC tissues as compared with NATs (Supplementary Figs. S1B–S1D). Among these 11 circRNAs, circARFGEF2 was most significantly upregulated in *KRAS*^{G12D} PDAC tissues as compared with PDAC tissues with other *KRAS* subtypes (*KRAS*^{G12C}, *KRAS*^{G12V}, *KRAS*^{WT}; **Fig. 1A** and **B**; Supplementary Fig. S1E).

Moreover, circARFGEF2 was overexpressed in LN-positive patients with *KRAS*^{G12D} PDAC or patients with a highly pathologic tumor-node-metastasis (TNM) stage, and the metastatic LNs possessed higher circARFGEF2 expression compared with the primary tumors (**Fig. 1C** and **D**; Supplementary Table S1). *In situ* hybridization (ISH) and immunofluorescence analysis revealed that circARFGEF2 overexpression was accompanied with increased microlymphatic vessel density (MLD) in *KRAS*^{G12D} PDAC tissues (**Fig. 1E** and **F**). Furthermore, fluorescence *in situ* hybridization (FISH) revealed circARFGEF2 enrichment in LN-positive *KRAS*^{G12D} PDAC tissues compared with LN-negative (**Fig. 1G** and **H**), indicating that circARFGEF2 was positively correlated with LN metastasis of *KRAS*^{G12D} PDAC. Kaplan–Meier survival analysis demonstrated that circARFGEF2 overexpression was negatively correlated with overall survival (OS) and disease-free survival (DFS) in patients with *KRAS*^{G12D} PDAC (**Fig. 1I** and **J**). Univariate and multivariate Cox analysis indicated that circARFGEF2 was an independent prognostic factor of the OS and DFS of patients with *KRAS*^{G12D} PDAC (Supplementary Tables S2 and S3). In addition, circARFGEF2 was rarely differentially expressed or correlated with LN metastasis of other common cancers with *KRAS*^{G12D} mutation, including colon cancer and lung adenocarcinoma (Supplementary Figs. S1F–S1I), suggesting that the role of circARFGEF2 in *KRAS*^{G12D}-induced LN metastasis is specific to PDAC. Taken together, these results suggest that circARFGEF2 is positively associated with *KRAS*^{G12D} PDAC LN metastasis.

As the circular construction of circRNA determines their biological functions (12), we investigated the characteristics of circARFGEF2. We found that circARFGEF2 was derived from the back-splicing of exon 4 to 6 of the *ARFGEF2* gene (chr20:47567859–47570327; Supplementary Fig. S1J). Moreover, circARFGEF2 was detected in PCR products using complementary DNA (cDNA) as the template rather than genomic DNA (gDNA; **Fig. 1K**; Supplementary Fig. S1K). In addition, circARFGEF2 could only be amplified from the reverse transcription products of random primers instead of oligo-dT primers, confirming the circular form of circARFGEF2 without poly-A tail (**Fig. 1L**; Supplementary Fig. S1L). Furthermore, circARFGEF2 exhibited stronger resistance to RNase R compared with *ARFGEF2* mRNA, while actinomycin D assay demonstrated that circARFGEF2 had a longer half-life than *ARFGEF2* mRNA (**Fig. 1M** and **N**; Supplementary Figs. S1M and S1N), indicating that circARFGEF2 was more stable than *ARFGEF2* mRNA. Taken together, these findings demonstrate that circARFGEF2 has a highly stable structure.

QKI subset accelerates circARFGEF2 biogenesis in KRAS^{G12D} PDAC

We verified that circARFGEF2 abundance was increased in *KRAS*^{G12D} PDAC tissues compared with other *KRAS* subtypes. Subsequently, to examine whether circARFGEF2 upregulation in *KRAS*^{G12D} PDAC was a consequence of active regulation or alteration of the parent gene expression, we quantified circARFGEF2, *ARFGEF2* mRNA, and *ARFGEF2* pre-mRNA expression in *KRAS*^{G12D} PDAC.

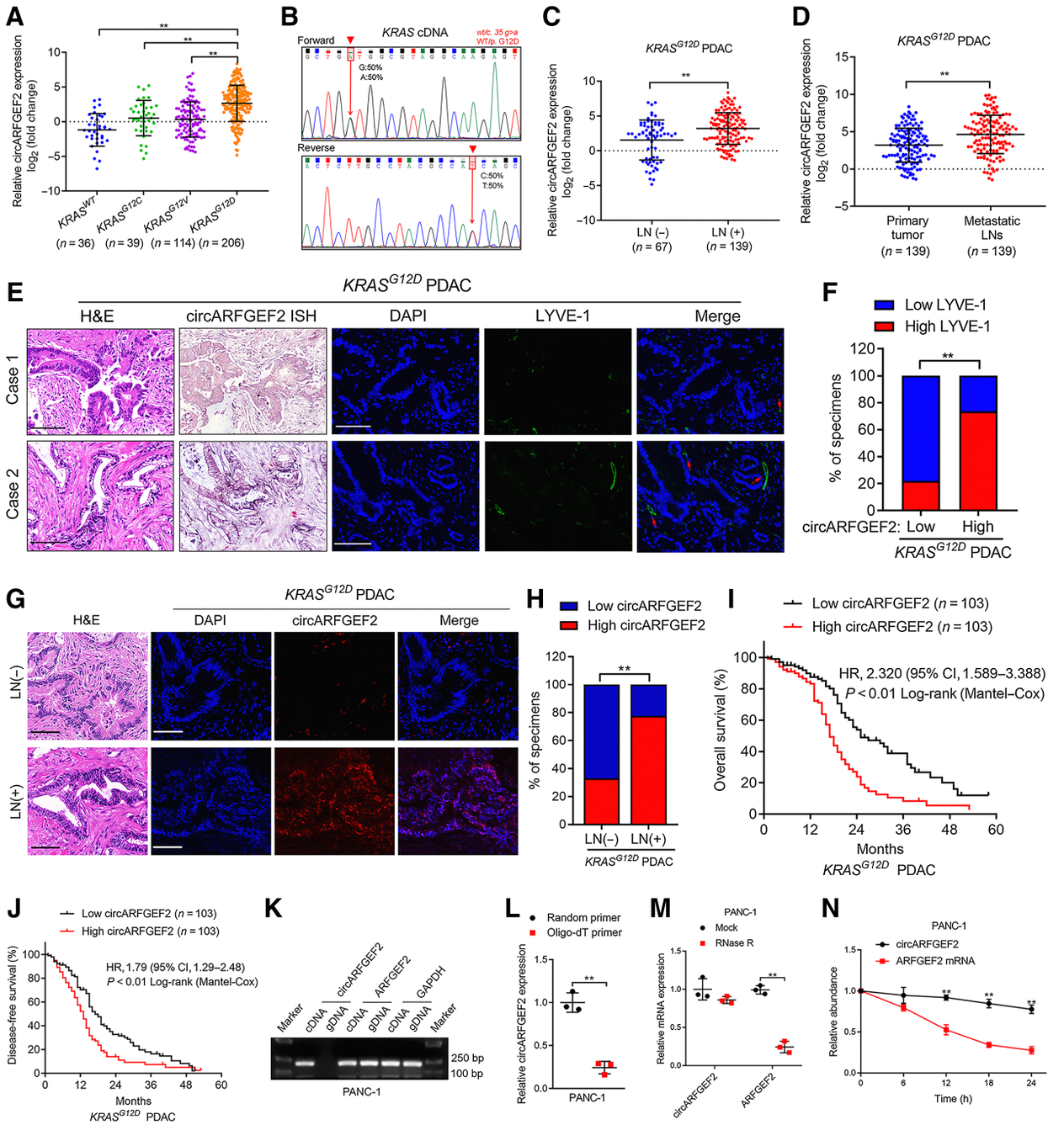

Figure 1.

Identification of circARFGEF2 in LN metastatic *KRAS*^{G12D} PDAC. **A,** qRT-PCR analysis of circARFGEF2 expression in the tumor tissues of patients with PDAC according to *KRAS* subtype (*KRAS*^{WT}, $n = 36$; *KRAS*^{G12C}, $n = 39$; *KRAS*^{G12V}, $n = 114$; *KRAS*^{G12D}, $n = 206$). The nonparametric Mann–Whitney *U* test was used. **B,** Sequencing evaluation of the *KRAS*^{G12D} mutations. **C,** qRT-PCR analysis of circARFGEF2 expression in LN-positive ($n = 139$) and LN-negative ($n = 67$) *KRAS*^{G12D} PDAC tissues. The nonparametric Mann–Whitney *U* test was used. **D,** qRT-PCR analysis of circARFGEF2 expression in the primary tumors and metastatic LNs of *KRAS*^{G12D} PDAC ($n = 139$). The nonparametric Mann–Whitney *U* test was used. **E** and **F,** Representative images (**E**) and percentages (**F**) of circARFGEF2 expression and LYVE-1–indicated lymphatic vessels in PDAC tissues. Scale bars, 50 μm. The χ^2 test was used. **G** and **H,** Representative images (**G**) and percentages (**H**) of circARFGEF2 expression in LN-positive or LN-negative *KRAS*^{G12D} PDAC tissues. Scale bars, 50 μm. The χ^2 test was used. **I** and **J,** Kaplan–Meier survival analysis of the OS (**I**) and DFS (**J**) of patients with PDAC with low versus high circARFGEF2 expression. The cut-off was the median. The nonparametric Mann–Whitney *U* test was used. **K,** PCR with agarose gel electrophoresis assay of circARFGEF2 and *ARFGEF2* in the cDNA and gDNA of PANC-1 cells. **L,** qRT-PCR analysis of circARFGEF2 expression using random primers or oligo-dT primers in PANC-1 cells. The two-tailed Student *t* test was used. **M,** qRT-PCR analysis of circARFGEF2 and *ARFGEF2* in PANC-1 cells treated with or without RNase R. The two-tailed Student *t* test was used. **N,** Assessment of circARFGEF2 and *ARFGEF2* stability in PANC-1 cells. The two-tailed Student *t* test was used. Error bars, SD from three independent experiments. **, $P < 0.01$. H&E, hematoxylin and eosin.

circARFGEF2 expression was significantly increased in the *KRAS*^{G12D} PDAC tissues compared with other *KRAS* subtypes (**Fig. 1A**), whereas *ARFGEF2* pre-mRNA expression was not significantly altered (Supplementary Fig. S2A), indicating that substantially more circARFGEF2 was present in *KRAS*^{G12D} PDAC. Importantly, the ratio of circARFGEF2 and *ARFGEF2* mRNA was increased in *KRAS*^{G12D} PDAC compared with other *KRAS* subtypes (Supplementary Fig. S2B), suggesting increased circARFGEF2 biogenesis in *KRAS*^{G12D} PDAC. To confirm this, we constructed a dual-color fluorescence reporter with circRNAs give rise to IRES-mediated translation of GFP and linear mRNA undergoes to mCherry to quantify linear and circRNA splicing of *ARFGER2* pre-mRNA simultaneously (**Fig. 2A**). The illustration of dual color fluorescence reporter assay was shown in Supplementary Fig. S9. Linear *ARFGEF2* generation indicated by HA-mCherry expression was increased and circARFGEF2 formation indicated by FLAG-GFP expression as well as GFP–mCherry ratio were significantly diminished after applying *KRAS*^{G12D} inhibitor MRTX1133 or *KRAS*^{G12D} siRNA in PANC-1 cells, whereas no obvious change was observed after applying MRTX1133 in Mia PaCa-2 (*KRAS*^{G12C}) and BxPC-3 (*KRAS*^{WT}) cells (**Fig. 2B–D**; Supplementary Figs. S2C–S2I), indicating that *KRAS*^{G12D} mutation is required for circARFGEF2 biogenesis.

The crucial role of QKI in circRNA biogenesis has been demonstrated previously (27). Accordingly, we performed next-generation sequencing in three paired *KRAS*^{G12D} PDAC tissues and NATs to evaluate whether QKI regulates circARFGEF2 biogenesis in *KRAS*^{G12D} PDAC and determined that QKI was upregulated in *KRAS*^{G12D} PDAC tissues (GSE234927; **Fig. 2E**). Dual-color fluorescence reporter assay showed that downregulating QKI expression significantly decreased the GFP–mCherry ratio (**Fig. 2F** and **G**), indicating that QKI is required for circARFGEF2 biogenesis.

QKI comprises three isoforms (QKI-5, QKI-6, QKI-7) that contribute to different RNA processing (28). To confirm the specific isoform that contributed to circARFGEF2 biogenesis in *KRAS*^{G12D} PDAC, dual-color fluorescence report assay and Western blotting assay were conducted and revealed that reducing QKI-5 expression significantly decreased FLAG-GFP expression while increased HA-mCherry expression (**Fig. 2H**; Supplementary Fig. S2J). Moreover, QKI-5 was significantly overexpressed in *KRAS*^{G12D} PDAC cells, rather than PDAC cells with other *KRAS* subtypes (Supplementary Fig. S2K). Increasing QKI-5 expression promoted circARFGEF2 expression in the PDAC cells while reducing QKI-5 expression diminished circARFGEF2 expression (Supplementary Figs. S2L–S2N), suggesting that QKI-5 was involved in circARFGEF2 biogenesis. We further explored the mechanism underlying *KRAS*^{G12D} mutation-induced QKI-5 overexpression. Given that *KRAS*^{G12D} mutation activated RAF/MEK/ERK, PI3K/AKT, and RAL/TBK1 signaling pathways to promote target genes expression in cancers (29, 30), we investigated whether these pathways were involved in *KRAS*^{G12D}-mediated QKI-5 overexpression. Inhibiting RAF/MEK/ERK signaling pathway with MCP110 significantly reduced QKI-5 expression, whereas neither inhibiting PI3K/AKT with LY294002 nor inhibiting RAL/TBK1 with BQU57 affected QKI-5 expression in PANC-1 cells (Supplementary Figs. S2O and S2P). Moreover, blocking *KRAS*^{G12D} mutation signaling decreased QKI-5 expression in PANC-1 cells, which was reversed by the activation of RAF/MEK/ERK with C16-PAF (Supplementary Figs. S2Q and S2R), indicating that RAF/MEK/ERK signaling pathway was required for *KRAS*^{G12D} mutation-induced QKI-5 expression. Together, these results suggest that *KRAS*^{G12D} mutation-driven QKI-5 overexpression promoted circARFGEF2 biogenesis in PDAC.

QKI-5 binds to the flanking introns of circARFGEF2 splicing exons

We investigated the mechanism underlying QKI-5-regulated circARFGEF2 biogenesis. It is well known that circRNA biogenesis is derived from pre-mRNA back-splicing (13). Thus, we investigated whether QKI-5 promotes circARFGEF2 biogenesis by regulating *ARFGEF2* pre-mRNA splicing. The results demonstrated that upregulated QKI-5 expression increased the circARFGEF2-*ARFGEF2* pre-mRNA ratio whereas decreased the *ARFGEF2* mRNA-*ARFGEF2* pre-mRNA ratio, indicating that QKI-5 regulated *ARFGEF2* pre-mRNA splicing (Supplementary Fig. S3A). Pre-mRNA alternative splicing is generally catalyzed by spliceosome, the assembly of which occurs stepwise along with associated protein cofactors. Coimmunoprecipitation assays followed by MS and Western blotting identified that the QKI-5 interacted with U2 auxiliary factor 1 (U2AF35), a U2AF subunit that directly triggers spliceosome assembly to stimulate splicing (**Fig. 2I** and **J**). Moreover, decreasing U2AF35 expression significantly impeded QKI-5-induced circARFGEF2 biogenesis (**Fig. 2K** and **L**). The above results indicate that QKI-5 recruits U2AF35 to regulate *ARFGEF2* pre-mRNA splicing and promote circARFGEF2 biogenesis.

The effect of QKI-5 on circRNA formation occurred through direct binding with the binding sites on pre-mRNAs (20). RIP was performed to determine that QKI-5 directly bound to *ARFGEF2* pre-mRNA (Supplementary Fig. S3B). Because it is well defined that RBPs bind to the flanking introns of circRNA splicing exons and induce circularization, we designed primers for the introns adjacent to circARFGEF2-forming exons and found that QKI-5 bound to the exon-adjacent sites (intron 3 and 6) at much higher level compared with more distal regions elsewhere in *ARFGEF2* pre-mRNA (Supplementary Fig. S3C).

To confirm the precise QKI-5 binding sites on *ARFGEF2* pre-mRNA, we conducted pulldown assays with truncated sequences of intron 3 and 6, which revealed that QKI-5 was particularly enriched by intron $3^{1000–1200\ nt}$ and intron $6^{7600–7800\ nt}$ (**Fig. 2M** and **N**; Supplementary Figs. S3D and S3E). Moreover, RBPmap revealed a reverse complement sequence neighboring the QKI binding motifs at intron $3^{1128–1180\ nt}$ and intron $6^{7672–7740\ nt}$ (Supplementary Figs. S3F–S3I). Mutation of intron $3^{1128–1180\ nt}$ and intron $6^{7672–7740\ nt}$ impaired QKI-5 and *ARFGEF2* pre-mRNA binding, suggesting that QKI-5 directly bound to these two *ARFGEF2* pre-mRNA regions (**Fig. 2O** and **P**). Furthermore, we assessed whether the interaction between QKI-5 and *ARFGEF2* pre-mRNA affected circARFGEF2 production in PDAC. CRISPR/Cas9-mediated knockout of intron $3^{1128–1180\ nt}$ and intron $6^{7672–7740\ nt}$ in *ARFGEF2* pre-mRNA substantially reduced QKI-5-mediated circARFGEF2 overexpression (**Fig. 2Q**; Supplementary Fig. S3J). Moreover, knocking out the QKI-5 binding sites on *ARFGEF2* pre-mRNA significantly diminished the rescue effect of U2AF35 on QKI-5 induced circARFGEF2 overexpression (Supplementary Figs. S3K and S3L). Together, our results demonstrate that QKI-5 recruits U2AF35 and binds to intron $3^{1128–1180\ nt}$ and intron $6^{7672–7740\ nt}$ in *ARFGEF2* pre-mRNA to promote circARFGEF2 splicing (**Fig. 2R**).

Increased circARFGEF2 biogenesis promotes KRAS^{G12D} PDAC lymphangiogenesis

As we observed a close clinical relationship between QKI-5-mediated circARFGEF2 expression and *KRAS*^{G12D} PDAC LN metastasis, we explored the biological function of QKI-5-mediated circARFGEF2 in *KRAS*^{G12D} PDAC *in vitro*. Lymphangiogenesis compounds the rate-limiting process of PDAC LN metastasis and we cocultured HLECs with PDAC cell culture medium to evaluate the role of circARFGEF2

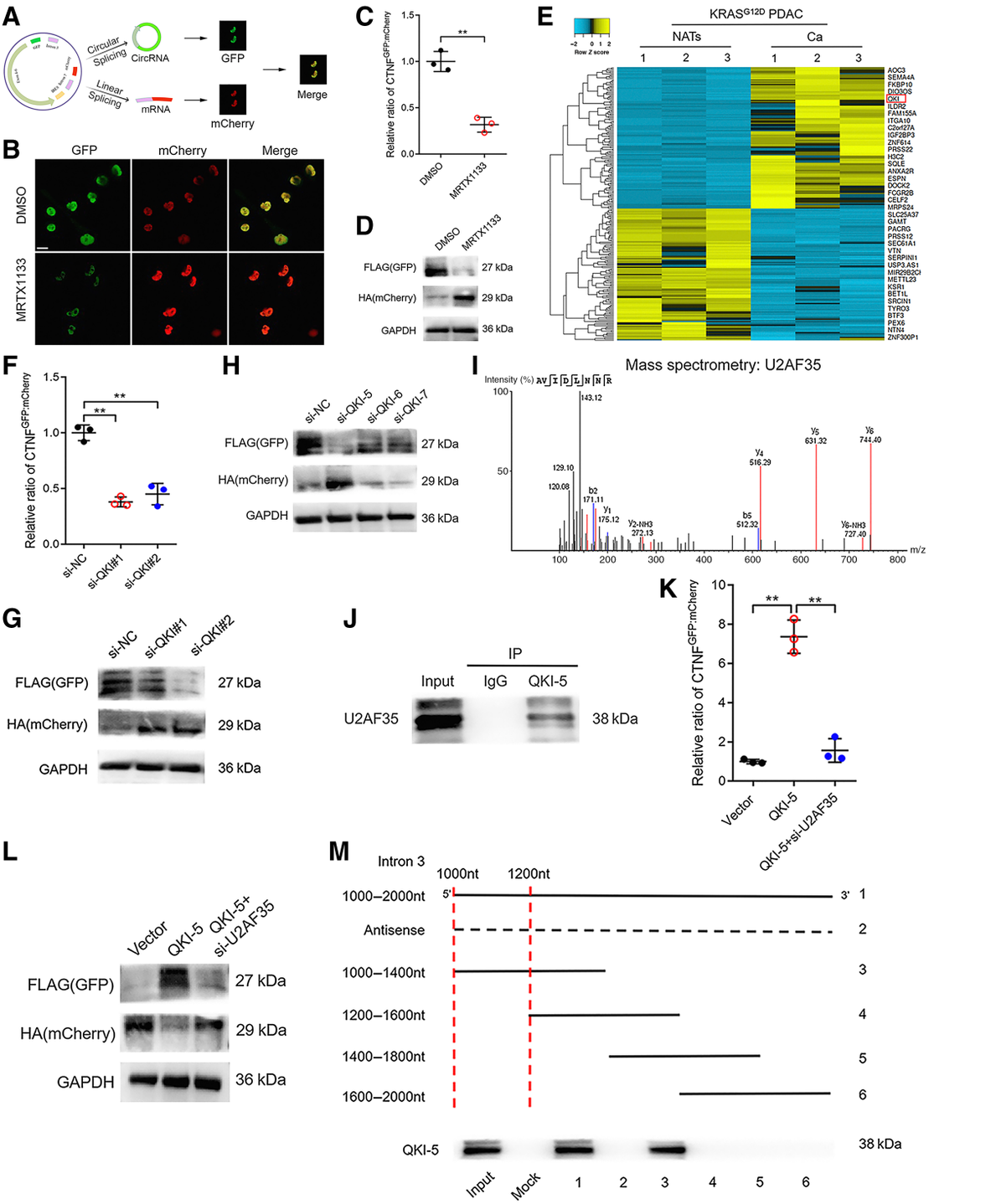

Figure 2.

QKI subset binds to the flanking introns of circARFGEF2 splicing exons and accelerates circARFGEF2 biogenesis in *KRAS*^{G12D} PDAC. **A,** Schematic illustration of the dual color fluorescence reporter. **B** and **C,** Representative images (**B**) and quantification (**C**) of circARFGEF2 and *ARFGEF2* mRNA expression in PDAC cells. Scale bars, 5 μm. The two-tailed Student *t* test was used. **D,** Western blotting analysis of GFP (FLAG-tagged) and mCherry (HA-tagged) expressions after *KRAS*^{G12D} inhibition in PDAC cells. **E,** Heat map of proteins differentially expressed in *KRAS*^{G12D} PDAC tissues and NATs. **F,** Relative expression ratio of circARFGEF2 and *ARFGEF2* mRNA after QKI downregulation in *KRAS*^{G12D} PDAC cells. **G,** Western blotting analysis of GFP (FLAG-tagged) and mCherry (HA-tagged) expression after QKI downregulation in *KRAS*^{G12D} PDAC cells. **H,** Western blotting analysis of GFP (FLAG-tagged) and mCherry (HA-tagged) expression after downregulating QKI-5, QKI-6, and QKI-7 in *KRAS*^{G12D} PDAC cells. **I,** MS analysis of the QKI-5-binding protein U2AF35 after coimmunoprecipitation assay. **J,** Western blotting analysis of the interaction between QKI-5 and U2AF35. **K,** Relative expression ratio of circARFGEF2 and *ARFGEF2* mRNA in *KRAS*^{G12D} PDAC cells. **L,** Western blotting analysis of GFP (FLAG-tagged) and mCherry (HA-tagged) expression in *KRAS*^{G12D} PDAC cells. (*Continued on the following page.*)

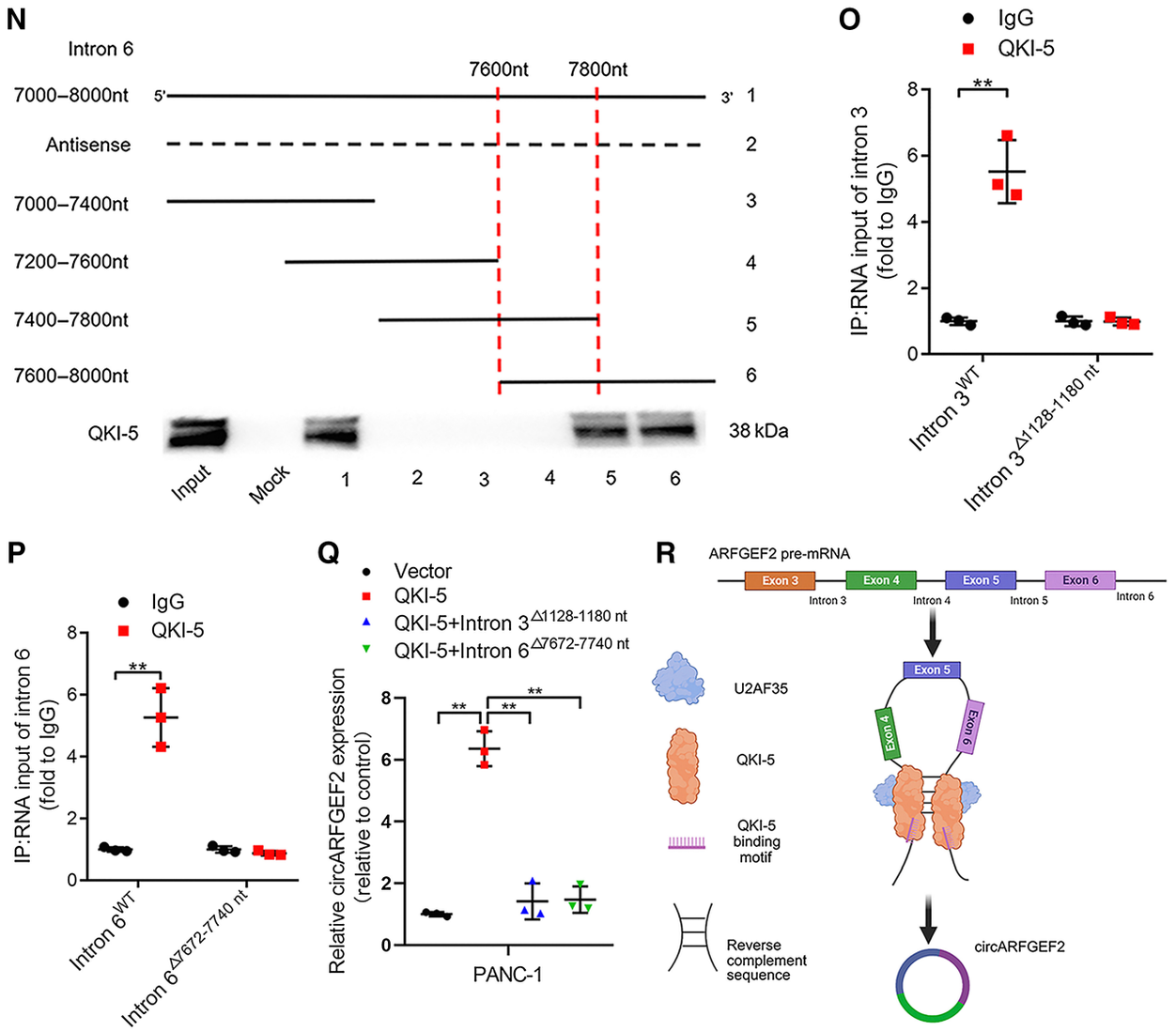

Figure 2.

(*Continued.*) **M** and **N,** Truncated sequences of intron 3 (**M**) and intron 6 (**N**) were used in RNA pulldown assays to identify the regions required for QKI-5 interaction. **O** and **P,** RIP performed after site-directed mutagenesis of intron $3^{1128–1180\ nt}$ (**O**) and intron $6^{7672–7740\ nt}$ (**P**) in PDAC cells. The two-tailed Student *t* test was used. **Q,** qRT-PCR analysis of circARFGEF2 expression in PANC-1 cells after QKI-5 overexpression or knockout of the QKI-5 binding sites in intron 3 and 6. One-way ANOVA followed by Dunnett test was used. **R,** Schematic illustration of QKI-5-mediated circARFGEF2 splicing. Error bars, SD from three independent experiments. **, $P < 0.01$. (**A**, Created with Figdraw).

in lymphangiogenesis (31, 32). The HLECs cocultured with cell culture medium of *KRAS*^{G12D} PDAC cells with higher circARFGEF2 expression had an increased tendency of tube formation and migration compared with those incubated with culture medium of PDAC cells with other *KRAS* subtypes, which possessed relatively lower circARFGEF2 expression (Supplementary Figs. S4A–S4C). Moreover, circARFGEF2 downregulation in *KRAS*^{G12D} PDAC cells suppressed HLEC tube formation and migration ability, whereas circARFGEF2 overexpression promoted *KRAS*^{G12D} PDAC cell-induced HLEC tube formation and migration (**Fig. 3A** and **B**; Supplementary Figs. S4D and S4E). 5-Ethynyl-2′-deoxyuridine (EDU) and Cell Counting Kit-8 (CCK8) assays showed that circARFGEF2 upregulation significantly increased the proliferation ability of HLECs, whereas circARFGEF2 downregulation exhibited the opposite effects (Supplementary Figs. S4F–S4I). Nevertheless, neither circARFGEF2 overexpression nor downregulation in PDAC cells with other *KRAS* subtypes affected HLEC tube formation and migration (Supplementary Figs. S5A–S5D). We further evaluated whether QKI-5 regulated the circARFGEF2-induced tube formation and migration in *KRAS*^{G12D} PDAC and demonstrated that QKI-5 overexpression enhanced HLEC tube formation and migration ability while downregulating circARFGEF2 expression suppressed the QKI-5-induced lymphangiogenesis of HLECs (**Fig. 3C**; Supplementary Fig. S5E). These findings suggest that QKI-5-mediated circARFGEF2 mainly promotes lymphangiogenesis of *KRAS*^{G12D} PDAC *in vitro*.

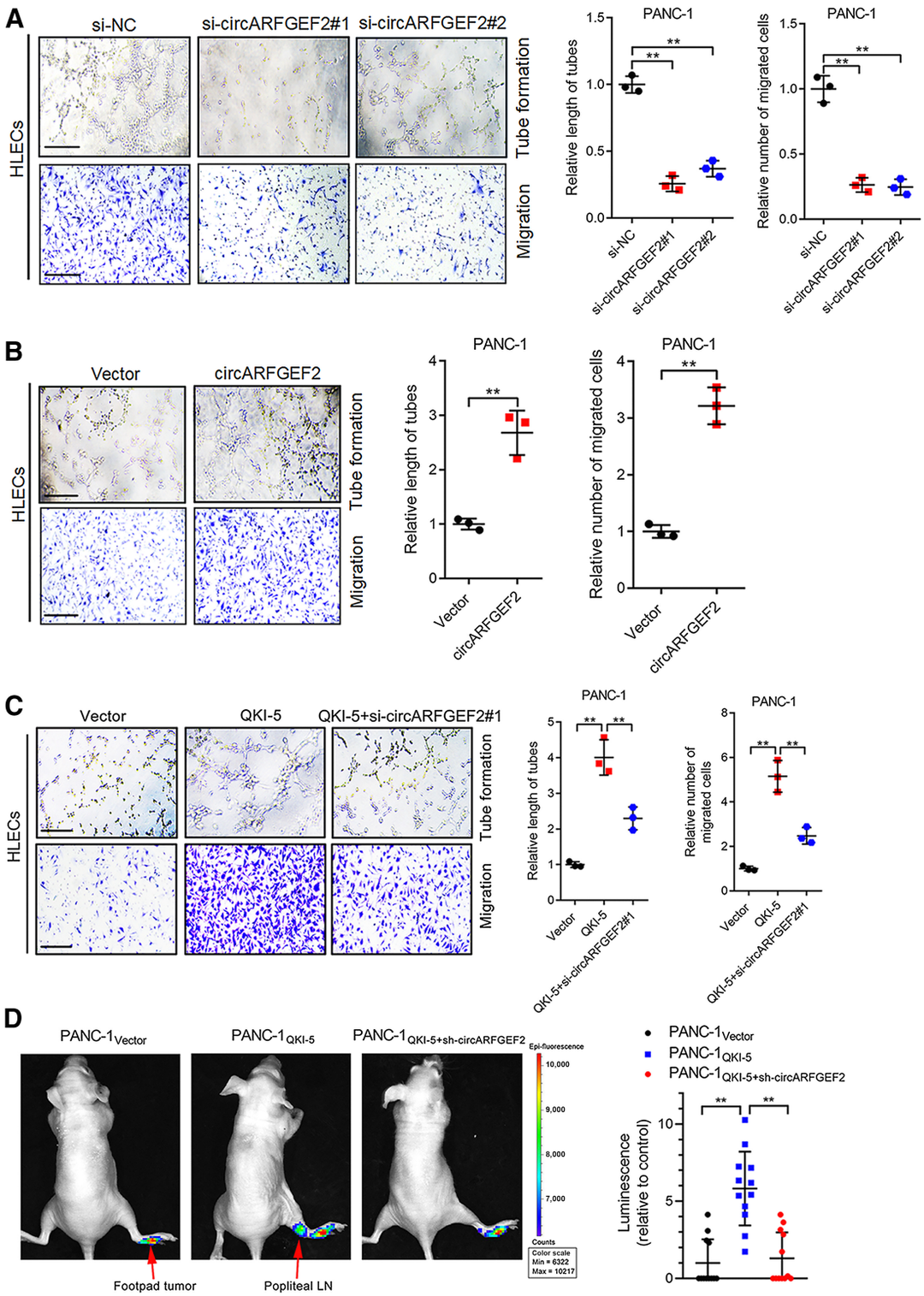

Figure 3.

Increased circARFGEF2 biogenesis promotes *KRAS*^{G12D} PDAC lymphangiogenesis *in vitro*. **A** and **B,** Representative images and quantification of tube formation and migration by HLECs treated with PANC-1 cell culture medium after circARFGEF2 knockdown (**A**) or overexpression (**B**). Scale bars, 100 μm. One-way ANOVA followed by Dunnett test was used. **C,** Representative images and quantification of tube formation and migration by HLECs cultured with the supernatant from PANC-1 cells with vector, QKI-5, or QKI-5+si-circARFGEF2#1. Scale bars, 100 μm. One-way ANOVA followed by Dunnett test was used. **D,** Representative images and quantification of popliteal metastatic LN bioluminescence ($n = 12$ per group). Arrows, footpad tumor and metastatic popliteal LNs. The two-tailed Student *t* test was used. (*Continued on the following page.*)

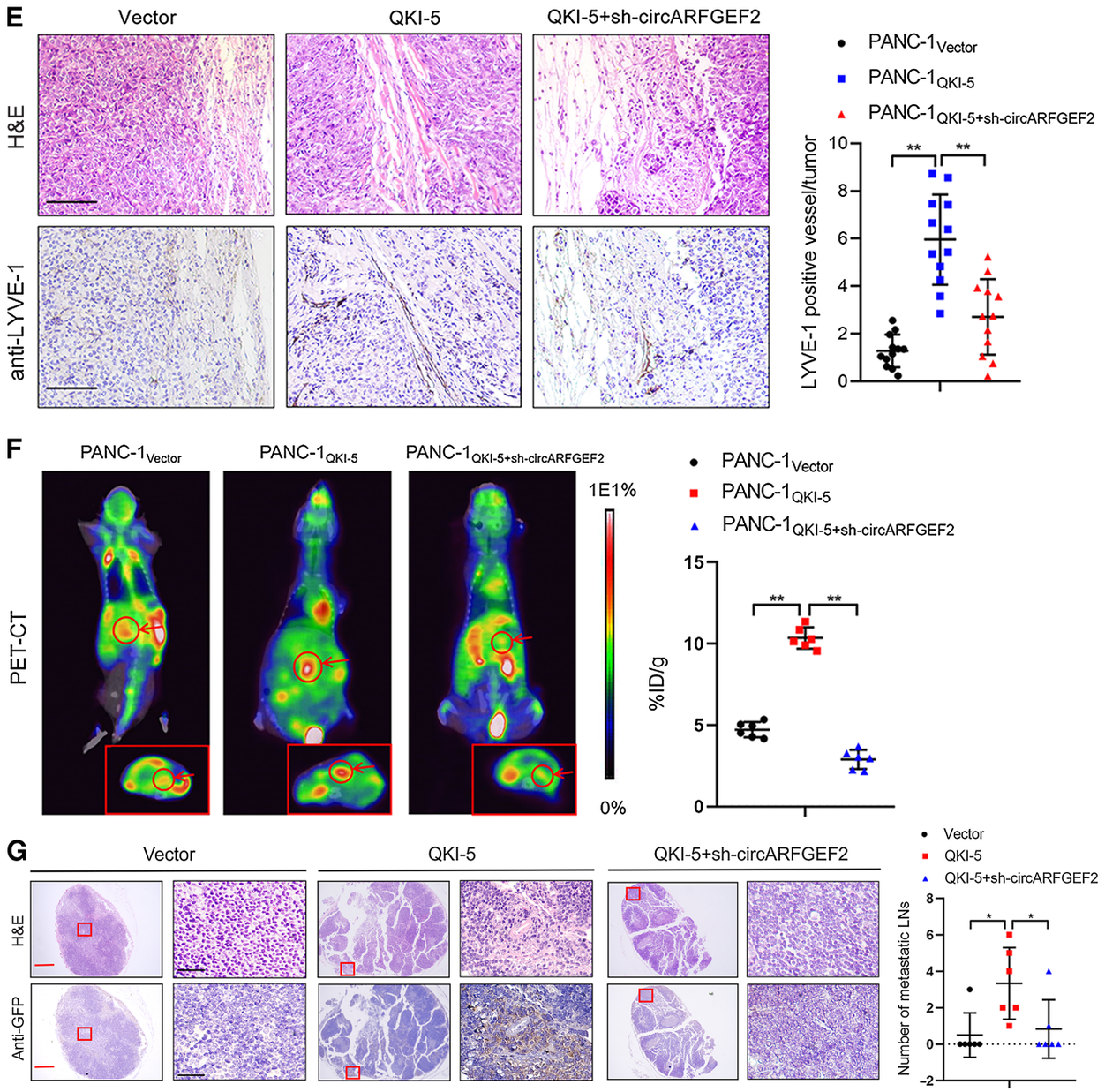

Figure 3.

(*Continued.*) **E,** Representative IHC images and quantification of LYVE-1–positive lymphatic vessel density in footpad tumors ($n = 12$ per group). Scale bar, 50 μm. The two-tailed Student *t* test was used. **F,** Representative PET-CT images of orthotopic tumors. The orthotopic pancreatic tumors in the coronal and transverse planes of the mouse are pointed out with red circles and arrows. ^{18F}FDG accumulation in the pancreas was assessed ($n = 6$ per group). ID, internalized dye. The two-tailed Student *t* test was used. **G,** Representative images of anti-GFP IHC analysis of nude mouse pancreatic LNs and quantification of the metastatic number of peri pancreatic LNs ($n = 6$ per group). Scale bars, 500 μm (red) and 50 μm (black). One-way ANOVA followed by Dunnett test was used. Error bars, SD from three independent experiments. *, $P < 0.05$; **, $P < 0.01$. H&E, hematoxylin and eosin.

Increased circARFGEF2 biogenesis promotes KRAS^{G12D} PDAC LN metastasis *in vivo*

To explore the effect of QKI-5-mediated circARFGEF2 on *KRAS*^{G12D} PDAC LN metastasis *in vivo*, we established popliteal LN metastasis models by injecting vector/GFP-, QKI-5/GFP- or QKI-5+sh-circARFGEF2/GFP-transfected PANC-1 cells into the foot pads of nude mice (Supplementary Fig. S5F). The LN status of the mice was monitored weekly with an In Vivo Imaging System (IVIS). QKI-5 overexpression significantly promoted the LN metastasis of *KRAS*^{G12D} PDAC cells, whereas downregulating circARFGEF2 obviously reversed this effect (**Fig. 3D**). IHC analysis of the primary tumors demonstrated that decreasing circARFGEF2 expression reversed the increment of MLD induced by QKI-5 upregulation (**Fig. 3E**). Moreover, QKI-5 overexpression shortened the mice survival whereas

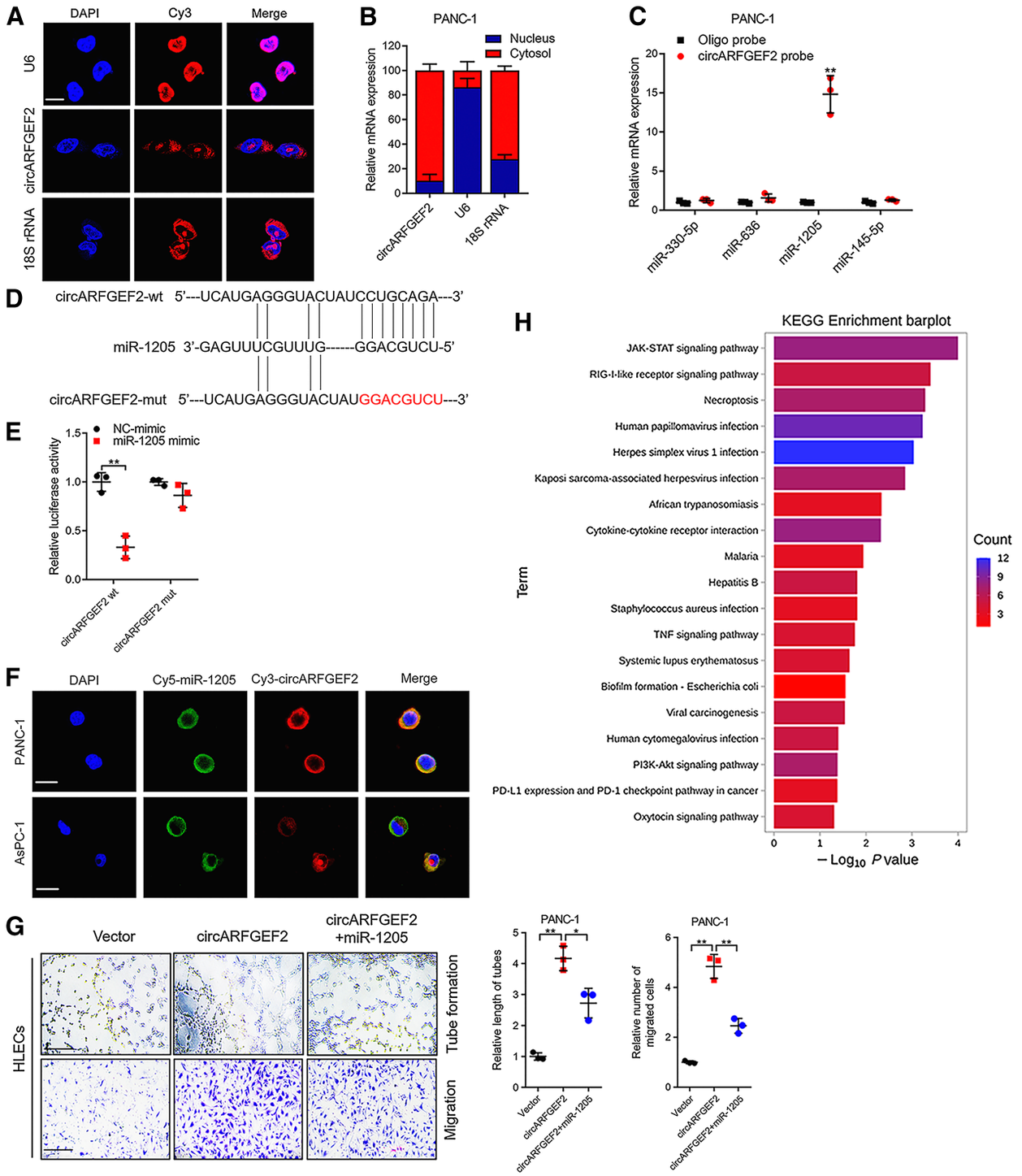

Figure 4.

QKI-5-mediated circARFGEF2 sponges miR-1205 and activates the JAK2–STAT3 signaling pathway in *KRAS*^{G12D} PDAC. **A** and **B,** Representative images (**A**) and quantification (**B**) of circARFGEF2 localization in PDAC cells. Scale bars, 5 μm. The χ^2 test was used. **C,** qRT-PCR analysis of the predicted miRNAs captured by circARFGEF2 probes in PANC-1 cells. The two-tailed Student *t* test was used. **D,** Schematic illustrating the sequence alignment of circARFGEF2 with miR-1205. **E,** Luciferase activities of the circARFGEF2-wt and circARFGEF2-mut plasmids quantified following PDAC cells transfected with negative control (NC) mimic or miR-1205 mimics. The two-tailed Student *t* test was used. **F,** Representative FISH images of circARFGEF2 and miR-1205 colocalization. Scale bar, 100 μm. **G,** Representative images and quantification of tube formation and migration by HLECs treated with PANC-1 cell culture medium. Scale bars, 100 μm. One-way ANOVA followed by Dunnett test was used. **H,** KEGG pathway analysis of enriched pathways in circARFGEF2-overexpressing PANC-1 cells. (*Continued on the following page.*)

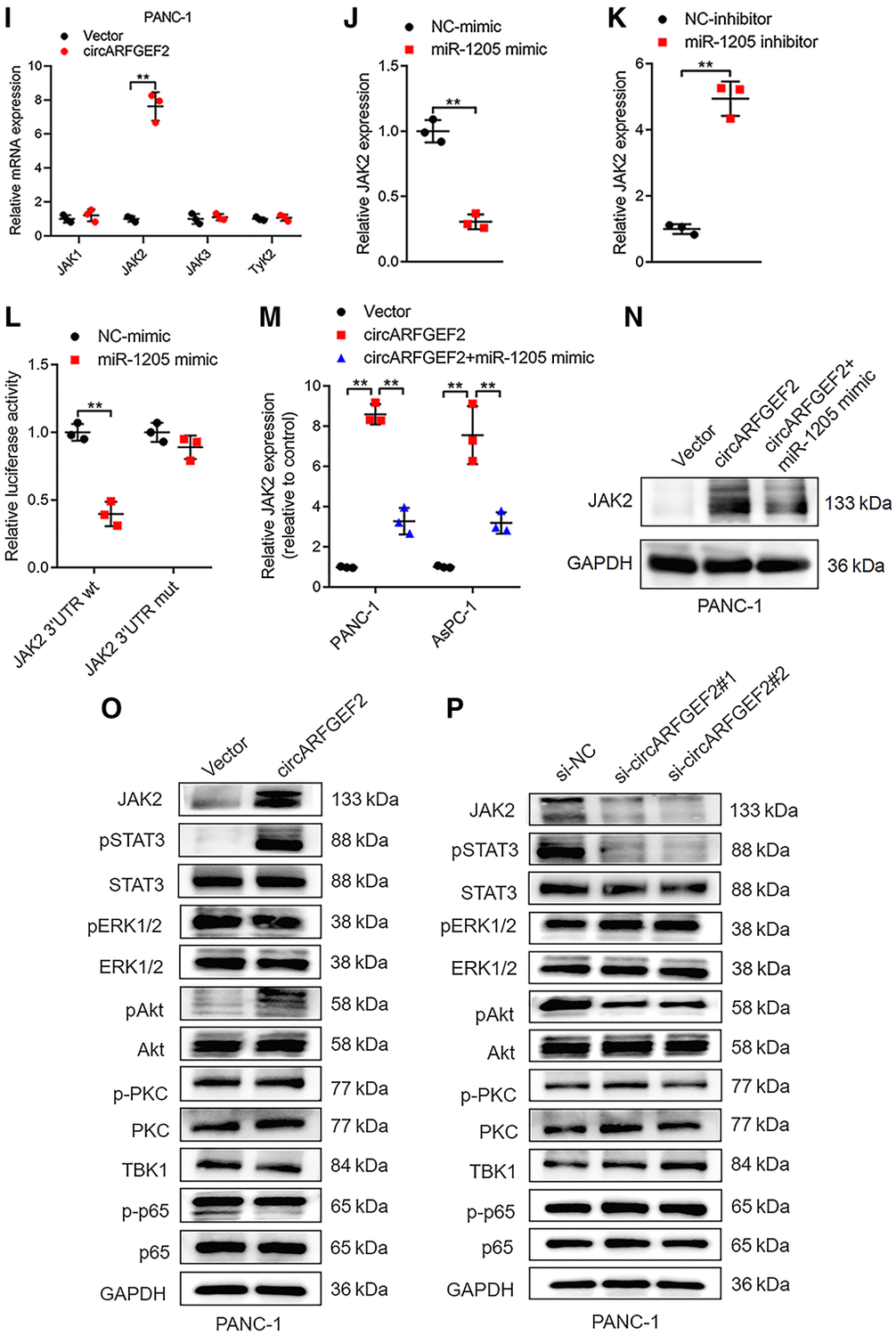

Figure 4.

(*Continued.*) **I,** qRT-PCR analysis of JAK–STAT signaling pathway-related genes after circARFGEF2 overexpression in PANC-1 cells. The two-tailed Student *t* test was used. **J** and **K,** qRT-PCR analysis of *JAK2* expression after miR-1205 overexpression (**J**) or downregulation (**K**). The two-tailed Student *t* test was used. **L,** Luciferase activities of the *JAK2* 3′UTR-wt and *JAK2* 3′UTR-mut plasmids quantified following PDAC cell transfected with NC mimic or miR-1205 mimics. The two-tailed Student *t* test was used. **M** and **N,** qRT-PCR (**M**) and Western blotting (**N**) analysis of JAK2 expression in PANC-1 and AsPC-1 cells transfected with vector, circARFGEF2, or circARFGEF2+miR-1205 mimic. The two-tailed Student *t* test was used. **O** and **P,** Western blotting analysis of crucial proteins of *KRAS* downstream effectors after circARFGEF2 overexpression (**O**) or downregulation (**P**). Error bars, SD from three independent experiments. *, $P < 0.05$; **, $P < 0.01$.

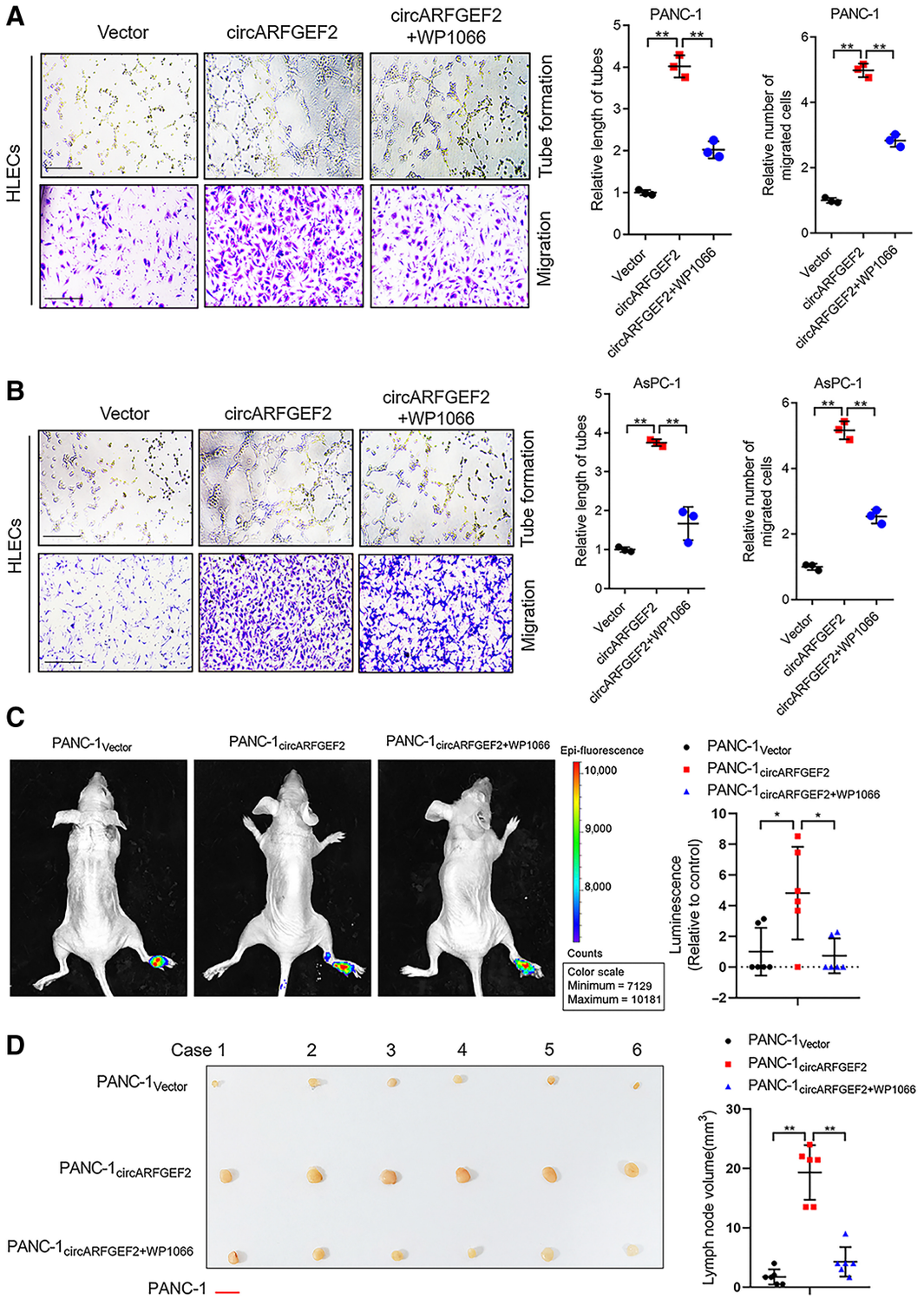

Figure 5.

QKI-5-mediated circARFGEF2 promotes *KRAS*^{G12D} PDAC lymphangiogenesis and LN metastasis via the JAK2–STAT3 pathway. **A** and **B,** Representative images and quantification of tube formation and migration by HLECs treated with culture medium from PANC-1 (**A**) and AsPC-1 (**B**) cells. Scale bars, 100 μm. One-way ANOVA followed by Dunnett test was used. **C,** Representative images and quantification of popliteal metastatic LNs bioluminescence ($n = 6$ per group). One-way ANOVA followed by Dunnett test was used. **D,** Representative images and quantification of popliteal LN volume. One-way ANOVA followed by Dunnett test was used ($n = 6$ per group). Scale bar, 0.5 cm. (*Continued on the following page.*)

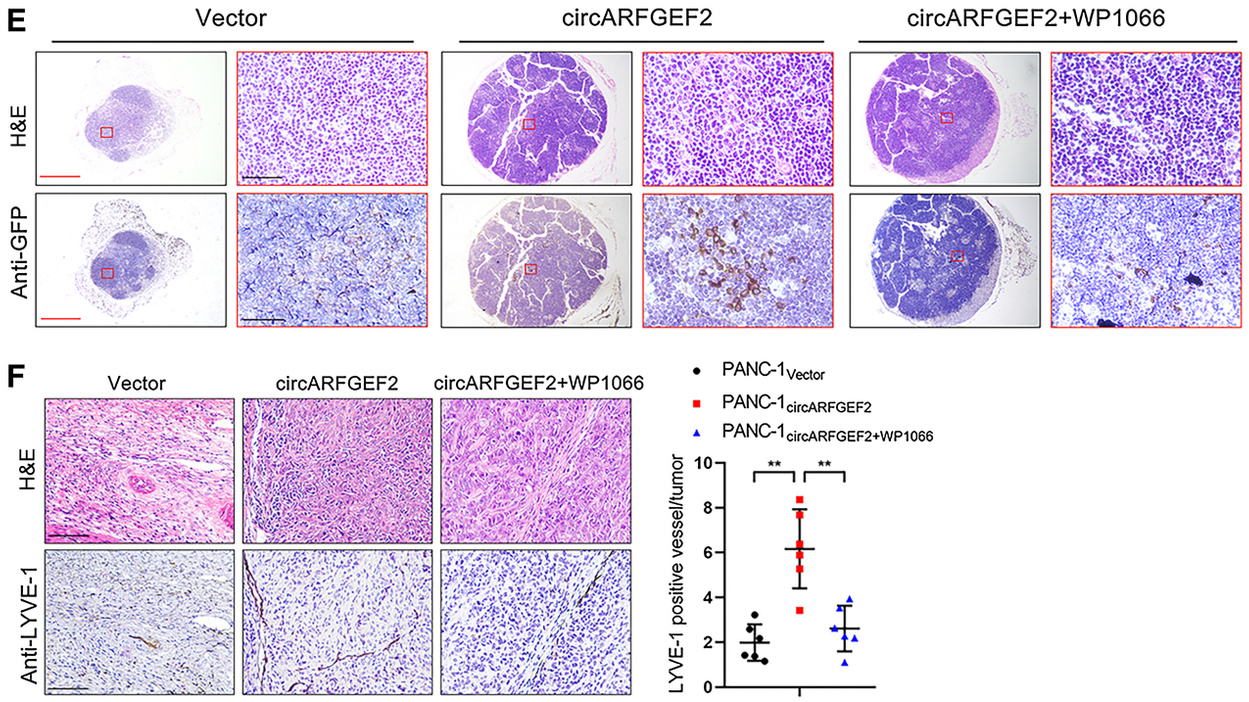

Figure 5.

(*Continued.*) **E,** Representative images of anti-GFP IHC analysis of nude mouse popliteal LNs (n = 6 per group). Scale bars, 500 μm (red) and 50 μm (black). **F,** Representative IHC images and quantification of LYVE-1-positive lymphatic vessel density in footpad tumors (n = 6 per group). Scale bar, 50 μm. One-way ANOVA followed by Dunnett test was used. Error bars, SD from three independent experiments. *, $P < 0.05$; **, $P < 0.01$. H&E, hematoxylin and eosin.

circARFGEF2 downregulation significantly reversed this effect (Supplementary Fig. S5G).

To simulate the anatomy and physiology of LN metastasis *in vivo*, we established the orthotopic xenograft model through implanting PANC-1 cells transfected with vector/GFP, QKI-5/GFP, and QKI-5+sh-circARFGEF2/GFP lentiviral plasmids into the pancreas of nude mice. PET-CT scanning was used to evaluate the orthotopic tumorigenicity of nude mice and the ^{18}F-fluorodeoxyglucose (^{18}FDG) accumulation of the orthotopic tumors in the pancreas were shown. The results showed that the PANC-1-QKI-5 group had higher accumulation of ^{18}FDG than the PANC-1-Vector group, while downregulating circARFGEF2 expression significantly reversed QKI-5-induced ^{18}FDG accumulation, suggesting that QKI-5 promoted the orthotopic tumorigenicity of *KRAS*^{G12D} PDAC cells and this effect was impeded when circARFGEF2 was downregulated (**Fig. 3F**). Given that the pyloric, hilar, and superior mesenteric LNs represent the most common drainage LNs of PDAC in mice, we enucleated these LNs to evaluate the metastasis of LNs (33). The results showed that QKI-5 significantly promoted the metastasis of cancer cells to peripancreatic LNs and increased the number of metastatic LNs in orthotopic xenograft PDAC model while decreasing circARFGEF2 expression reversed these effects (**Fig. 3G**). Taken together, the above results suggest that QKI-5-mediated circARFGEF2 promotes *KRAS*^{G12D} PDAC LN metastasis *in vivo*.

circARFGEF2 sponges miR-1205 in KRAS^{G12D} PDAC

We investigated the mechanism of circARFGEF2-induced *KRAS*^{G12D} PDAC LN metastasis. As circRNA localization within cells is crucial for their function (7), we conducted FISH and subcellular fractionation assays and found circARFGEF2 mainly located in the cytoplasm of *KRAS*^{G12D} PDAC cells (**Fig. 4A** and **B**; Supplementary Fig. S6A). Given that circRNAs located in the cytoplasm mainly sponge miRNAs, we explored the predicted binding miRNAs of circARFGEF2 with CircInteractome, miRanda, and RNAhybrid and found four miRNAs (hsa-miR-1205, hsa-miR-145–5p, hsa-miR-330–5p, and hsa-miR-636) to be potentially targeted by circARFGEF2 (Supplementary Fig. S6B). Among these miRNAs, miR-1205 was most specifically overexpressed in *KRAS*^{G12D} PDAC cell lines rather than PDAC cell lines with other *KRAS* subtypes (Supplementary Figs. S6C and S6D). RNA pulldown assay revealed that miR-1205 was significantly enriched by circARFGEF2 probes in the *KRAS*^{G12D} PDAC cells rather than *KRAS*^{WT} PDAC cells as compared with the Oligo probes (**Fig. 4C**; Supplementary Figs. S6E and S6F). Analysis of the circARFGEF2 and miR-1205 sequences revealed the existence of reverse complement sequences (**Fig. 4D**; Supplementary Fig. S6G). Dual luciferase reporter assay revealed that miR-1205 dramatically decreased the luciferase activity of the circARFGEF2 group, whereas the mutation of the reverse complement sequences impaired this effect (**Fig. 4E**; Supplementary Fig. S6H), suggesting that circARFGEF2 sponged miR-1205 via these specific sequences. Pulldown assay with miR-1205 probes demonstrated that miR-1205 specifically captured circARFGEF2 (Supplementary Fig. S6I). Furthermore, FISH assays demonstrated circARFGEF2 and miR-1205 colocalized in the cytoplasm of *KRAS*^{G12D} PDAC cells (**Fig. 4F**), indicating the interaction between circARFGEF2 and miR-1205.

Considering that circARFGEF2 acted as a miR-1205 sponge in *KRAS*^{G12D} PDAC cells, we investigated whether circARFGEF2 promoted *KRAS*^{G12D} PDAC lymphangiogenesis by sponging miR-1205.

In vitro experiments demonstrated that overexpressing circARFGEF2 triggered HLEC tube formation and migration, whereas overexpressing miR-1205 obviously reversed this effect (**Fig. 4G**; Supplementary Figs. S6J–S6L). Taken together, our results demonstrate that circARFGEF2 acts as a miR-1205 sponge in $KRAS^{G12D}$ PDAC cells.

circARFGEF2 activates the JAK2–STAT3 pathway in $KRAS^{G12D}$ PDAC

As circRNAs act as miRNA sponges to regulate downstream genes expression (34), we conducted mRNA transcriptome analysis in PANC-1 cells to identify the targets of circARFGEF2. Kyoto Encyclopedia of Genes and Genomes (KEGG) pathway analysis revealed that the JAK–STAT pathway was the most significantly enriched pathway associated with circARFGEF2 (**Fig. 4H**). JAK represents the core component for the activation the JAK–STAT pathway and consists of JAK1, JAK2, JAK3, and TYK2 (35, 36). Subsequently, we detected the expression profiles of the four JAK subtypes and found that JAK2 was positively associated with the expression of circARFGEF2 in $KRAS^{G12D}$ PDAC cells (**Fig. 4I**; Supplementary Fig. S6M). Moreover, miR-1205 was negatively associated with JAK2 expression in $KRAS^{G12D}$ PDAC cells (**Fig. 4J** and **K**). miRNAs regulate target genes expression mainly by binding to their 3′UTR (37). Analysis of the *JAK2* 3′UTR region revealed a sequence complementary to miR-1205 (Supplementary Fig. S7A). The dual luciferase reporter assays demonstrated that miR-1205 obviously decreased the luciferase activity in the *JAK2* 3′UTR luciferase construct rather than that with a mutant sequence in the miR-1205 binding site (**Fig. 4L**). miR-1205 overexpression obviously inhibited circARFGEF2-induced JAK2 expression, suggesting that circARFGEF2 acted as a miR-1205 sponge to increase JAK2 expression (**Fig. 4M** and **N**; Supplementary Fig. S7B). Western blotting assays revealed that circARFGEF2 overexpression promoted JAK2 expression and STAT3 phosphorylation (**Fig. 4O**; Supplementary Figs. S7C and S7D), whereas circARFGEF2 downregulating reduced JAK2 expression and inhibited STAT3 phosphorylation (**Fig. 4P**; Supplementary Figs. S7E and S7F), the full uncut gels of Western blotting were shown in Supplementary Fig. S10. In addition, we investigated the effect of circARFGEF2 on other *KRAS* downstream effectors, including ERK, AKT, PKCs, TBK1, and p65 (30, 38). Neither circARFGEF2 downregulation nor upregulation showed significant effect on the expression of ERK, AKT, PKC, TBK1, and p65 (Supplementary Figs. S7G and S7H), the primers are listed in Supplementary Table S4. Western blotting assays showed that circARFGEF2 was positively correlated with the phosphorylation of AKT (**Fig. 4O** and **P**), which was previously demonstrated as the downstream target of JAK2, the antibodies are listed in Supplementary Table S5 (39). Altogether, these findings demonstrate that circARFGEF2 sponges miR-1205 to upregulate JAK2 expression and activate the JAK2–STAT3 pathway in $KRAS^{G12D}$ PDAC.

Next, we further clarified whether JAK2–STAT3 pathway activation was indispensable for circARFGEF2-induced lymphangiogenesis and LN metastasis in $KRAS^{G12D}$ PDAC. circARFGEF2 overexpression significantly promoted HLEC tube formation and migration ability, whereas the JAK2–STAT3 pathway inhibitor WP1066 significantly reversed this effect (**Fig. 5A** and **B**). Furthermore, *in vivo* experiments demonstrated that the circARFGEF2-overexpressing nude mice had larger popliteal LNs compared with the control nude mice, and WP1066 significantly impeded the circARFGEF2-induced LN metastasis (**Fig. 5C** and **D**). IHC analysis revealed that circARFGEF2 overexpression promoted the metastasis of popliteal LNs and increased the MLD in the foot pad tumors, while inhibiting JAK2–STAT3 pathway reversed these effects (**Fig. 5E** and **F**). These results suggest that circARFGEF2 promotes lymphangiogenesis and LN metastasis in $KRAS^{G12D}$ PDAC via the JAK2-STAT3 pathway.

JAK2–STAT3 pathway inhibition suppresses circARFGEF2-induced LN metastasis in KPC mice

To better understand the role of circARFGEF2 in $KRAS^{G12D}$ PDAC LN metastasis *in vivo*, we used the engineered transgenic $Kras^{G12D/+}Trp53^{R172H/+}$Pdx-1-Cre (KPC) mouse, a well-characterized autochthonous model that develops the full spectrum of $KRAS^{G12D}$ mutation-induced PDAC (40, 41). The results showed that circARFGEF2 overexpression significantly increased primary PDAC tumor volume and inhibiting the JAK2–STAT3 signaling pathway reversed this effect (**Fig. 6A** and **B**). Moreover, circARFGEF2 overexpression significantly increased the number of metastatic abdominal LNs in KPC mice and the MLD in primary PDAC tumors, whereas blocking JAK2–STAT3 signaling pathway impeded these effects (**Fig. 6C** and **D**; Supplementary Fig. S7I). We also evaluated the effect of circARFGEF2 downregulation in the LN metastasis of KPC mouse with AAV-sh-circARFGEF2. PET-CT scanning was used to evaluate the tumorigenicity of PDAC tumors in KPC mice and the ^{18}FDG accumulation of the PDAC tumors in KPC mice were shown. The results of PET-CT scanning showed that downregulating circARFGEF2 expression obviously reduced ^{18}FDG accumulation in the PDAC tumors of KPC models compared with the control group (Supplementary Fig. S8A). Moreover, the number of metastatic LNs in sh-circARFGEF2 group was lower than sh-NC group (Supplementary Fig. S8B). Then we separated the PDAC tumors in KPC models and evaluated the MLD in PDAC tumors. HE and IHC results revealed that the MLD was significantly decreased in sh-circARFGEF2 group, indicating that circARFGEF2 downregulation impeded the lymphangiogenesis in the primary PDAC tumors of KPC models (Supplementary Figs. S8C and S8D). These results suggest that blockage of JAK2-STAT3 pathway exhibit a suppression effect on circARFGEF2-induced lymphangiogenesis and LN metastasis of $KRAS^{G12D}$ PDAC.

Clinical relevance of the QKI-5–circARFGEF2–JAK2 axis in patients with $KRAS^{G12D}$ PDAC

Given that QKI-5-mediated circARFGEF2 induced $KRAS^{G12D}$ PDAC lymphangiogenesis and LN metastasis by sponging miR-1205 and activating JAK2–STAT3 signaling pathway, we assessed the clinical significance of the QKI-5-mediated circARFGEF2–miR-1205–JAK2 axis in patients with $KRAS^{G12D}$ PDAC. The results demonstrated that miR-1205 was downregulated and circARFGEF2, QKI-5, JAK2 were upregulated in $KRAS^{G12D}$ PDAC tissues in comparison with the NATs (**Fig. 6E** and **F**; Supplementary Figs. S8E and S8F), and miR-1205 was upregulated in $KRAS^{G12D}$ PDAC tissues compared with PDAC tissues with other *KRAS* subtypes (Supplementary Fig. S8G). Moreover, miR-1205 was negatively associated with LN metastasis while circARFGEF2, QKI-5, and JAK2 were significantly upregulated in the LN metastatic $KRAS^{G12D}$ PDAC tissues (**Fig. 6G** and **H**; Supplementary Figs. S8H–S8J). In addition, we found no significant association between circARFGEF2 or miR-1205 expression and liver or lung metastasis in PDAC patients (Supplementary Figs. S8K–S8N). The above findings suggest that QKI-5-mediated circARFGEF2–miR-1205–JAK2 axis is specifically associated with LN metastasis of patients with PDAC.

IHC analysis revealed that QKI-5 and JAK2 were positively correlated with circARFGEF2 expression in the $KRAS^{G12D}$ PDAC tissues (**Fig. 6I**–**K**). Correlation analysis revealed that JAK2 was negatively associated with miR-1205 expression while positively associated with

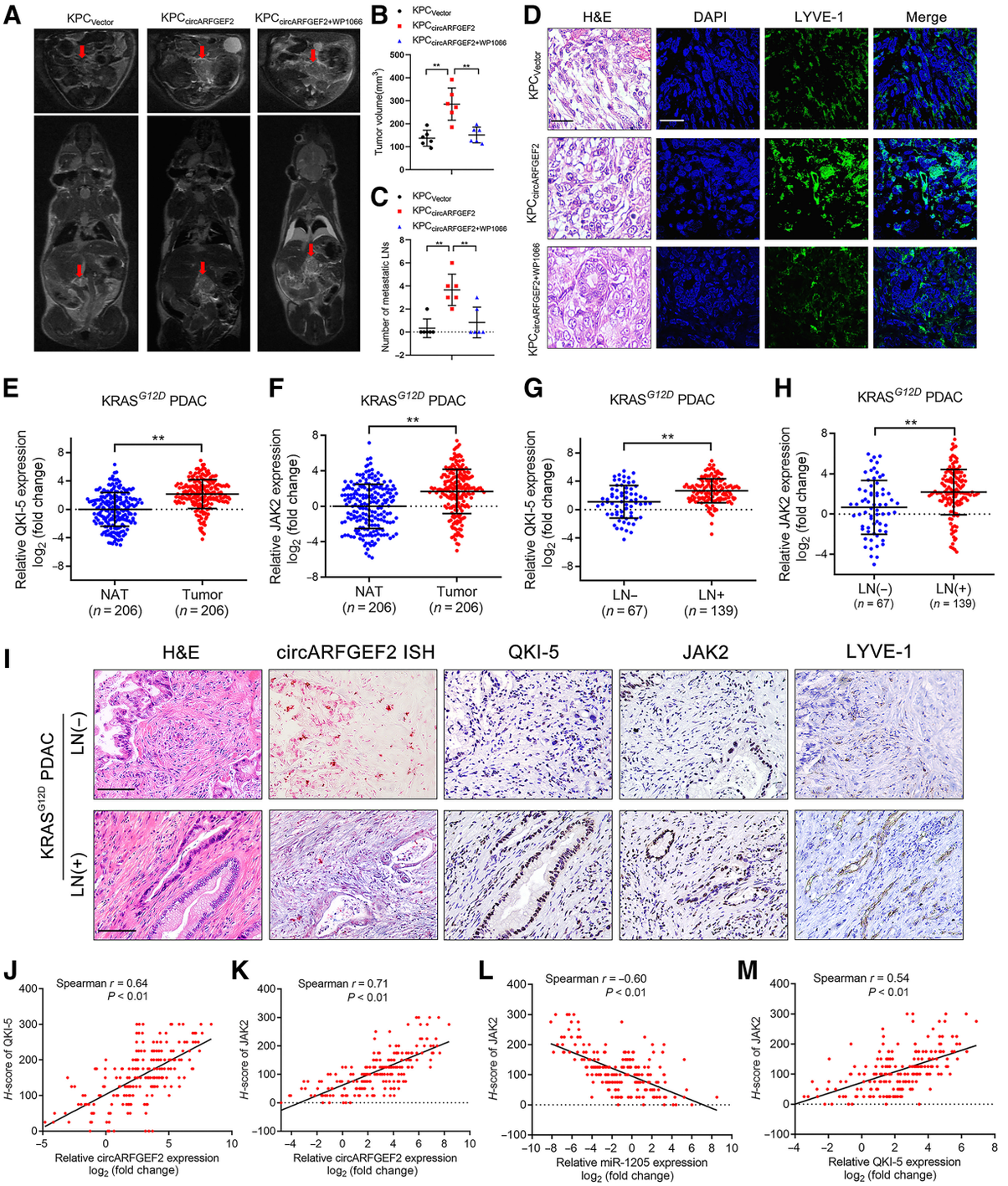

Figure 6.

Clinical relevance of the QKI-5-mediated circARFGEF2–miR-1205–JAK2 axis in *KRAS*^{G12D} PDAC. **A,** Representative images of MR images of KPC tumors. Red arrows, KPC tumor. **B,** Quantification of KPC tumor volume. One-way ANOVA followed by Dunnett test was used. **C,** Quantification of the metastatic number of peripancreatic LNs. One-way ANOVA followed by Dunnett test was used. **D,** Representative hematoxylin and eosin (H&E)-stained and immunofluorescence images of LYVE-1-positive lymphatic vessel density in KPC tumors. Scale bars, 50 μm. **E** and **F,** qRT-PCR analysis of QKI-5 (**E**) and JAK2 (**F**) expression in the tumor tissues and NATs from patients with *KRAS*^{G12D} PDAC ($n = 206$). The nonparametric Mann–Whitney *U* test was used. **G** and **H,** qRT-PCR analysis of QKI-5 (**G**) and JAK2 (**H**) expression in LN-positive ($n = 139$) and LN-negative ($n = 67$) *KRAS*^{G12D} PDAC tissues. The nonparametric Mann–Whitney *U* test was used. **I–M,** Representative images (**I**) of the association between circARFGEF2 expression and QKI-5, JAK2, and LYVE-1–positive lymphatic vessel density in LN-positive and LN-negative *KRAS*^{G12D} PDAC. The correlation between circARFGEF2 and QKI-5 (**J**), circARFGEF2 and JAK2 (**K**), miR-1205 and JAK2 (**L**), QKI-5 and JAK2 (**M**) was analyzed. Error bars, SD from three independent experiments. **, $P < 0.01$.

QKI-5 expression, and a negative correlation was observed between circARFGEF2 and miR-1205 expression (**Fig. 6L** and **M**; Supplementary Fig. S8O). The above results indicated the critical role of the QKI-5-mediated circARFGEF2–miR-1205–JAK2 axis in $KRAS^{G12D}$ PDAC LN metastasis. Together, our findings demonstrate that circARFGEF2 derived from QKI-5-dependent splicing sponged miR-1205 and activated the JAK2–STAT3 signaling pathway to induce $KRAS^{G12D}$ PDAC LN metastasis.

Discussion

Aberrant pre-mRNA splicing causes the production of alternative RNA variants, including circRNAs, and leads to human cancer stemness, proliferation, and metastasis (42). Nonetheless, the precise mechanism of circRNA production via pre-mRNA splicing in $KRAS^{G12D}$ PDAC LN metastasis remains unexplored. In this study, we determined that circARFGEF2 was overexpressed via a $KRAS^{G12D}$ mutant-related splicing in PDAC and triggered the lymphangiogenesis and LN metastasis of $KRAS^{G12D}$ PDAC cells both *in vitro* and *in vivo*.

We constructed a dual-color fluorescence reporter system to demonstrate that the circARFGEF2 biogenesis was significantly activated by the alternative splicing factor QKI-5. QKI-5 promoted circARFGEF2 biogenesis by recruiting U2AF35 and regulating *ARFGEF2* pre-mRNA back-splicing. Subsequently, circARFGEF2 sponged miR-1205 and activated the JAK2-STAT3 signaling pathway to induce $KRAS^{G12D}$ PDAC lymphangiogenesis and LN metastasis. Our study highlighted a mechanism of QKI-5-mediated circRNA production in regulating $KRAS^{G12D}$ PDAC LN metastasis, indicating that targeting circARFGEF2 production is a potential therapeutic strategy for LN metastatic PDAC with $KRAS^{G12D}$ mutation.

KRAS mutation is the most frequently mutated oncogene, occurring in approximately 90% of patients with PDAC, where $KRAS^{G12D}$ is the most common allele in PDAC (43). Recent studies revealed that $KRAS^{G12D}$ mutation caused the aberrant gene expression profile by regulating RNA processing to drive tumor progression (9, 17). However, the role of the $KRAS^{G12D}$ mutation in triggering the circRNA process during tumor development remains unknown. In this study, circRNA production was responsive to the $KRAS^{G12D}$ mutation in PDAC and was crucial in PDAC LN metastasis. Moreover, we demonstrated that the RNA splicing regulator QKI-5 was associated with $KRAS^{G12D}$ and revealed that the $KRAS^{G12D}$ mutation promoted circARFGEF2 biogenesis by triggering QKI-5-induced back-splicing of circARFGEF2. Targeting the $KRAS^{G12D}$ mutation with a specific inhibitor dramatically abolished circARFGEF2 production and its role in fostering PDAC LN metastasis. Our study clarified the precise mechanism underlying $KRAS^{G12D}$ mutation-induced circRNA production, suggesting a new perspective in $KRAS^{G12D}$ PDAC LN metastasis.

QKI is a potential regulator of pre-mRNA alternative splicing in developmental and pathologic processes. QKI has three major alternatively spliced isoforms (QKI-5, QKI-6, QKI-7) that differ at the carboxy-terminal end and contribute to different RNA-processing functions (28). QKI-5 is predominantly located in the nucleus and regulates pre-mRNA splicing (20, 21). QKI-6 and QKI-7 lack nuclear localization signals and regulate posttranscriptional mRNA processing, such as RNA stability and transportation (44, 45). Notably, all three isoforms regulate the biogenesis of certain circRNAs by regulating alternative pre-mRNA splicing (28, 46). Nevertheless, the specific isoform that regulates circRNA biogenesis in LN metastatic $KRAS^{G12D}$ PDAC is unclear. In this study, we determined that QKI-5 facilitated circARFGEF2 production in $KRAS^{G12D}$ PDAC by interacting with the splicing factor U2AF35. Moreover, U2AF35 assisted with QKI-5 in recognizing the intron $3^{1128–1180\ nt}$ and intron $6^{7672–7740\ nt}$ of *ARFGEF2* pre-mRNA, which benefited *ARFGEF2* pre-mRNA cyclization and back-splicing. Decreasing U2AF35 expression significantly impaired the binding between QKI-5 and the flanking introns of *ARFGEF2* pre-mRNA and inhibited circARFGEF2 biogenesis. Our study revealed the specific QKI-5 recognition and splicing pattern that regulated circARFGEF2 production in LN metastatic $KRAS^{G12D}$ PDAC, which expanded our understanding of QKI-5-mediated circRNA splicing.

circRNAs have been acknowledged as feasible therapeutic targets that exhibited satisfactory tumor suppression effects in mouse models, indicating the broad prospect of circRNAs in cancer treatment (47, 48). *KRAS* mutant cells exhibit different gene expression profiles, including circRNAs, according to a recent study (9). *KRAS*-responsive circRNAs promote target gene stabilization and control extracellular exportation to promote tumorigenesis (17). However, the relationship between circRNA biogenesis and $KRAS^{G12D}$ PDAC is still unclear. In our study, we discovered that circRNA biogenesis was strongly related to the $KRAS^{G12D}$ mutation in PDAC and was essential for the LN metastasis of PDAC. We identified circARFGEF2, a $KRAS^{G12D}$-responsive circRNA, was involved in $KRAS^{G12D}$-mediated LN metastasis of PDAC. The overproduction of circARFGEF2 was induced by a RNA splicing factor, QKI-5, which was overexpressed in $KRAS^{G12D}$ PDAC. Importantly, we determined that blocking QKI-5-induced circARFGEF2 biogenesis significantly inhibited $KRAS^{G12D}$ PDAC LN metastasis in the mice model. Thus, further developing therapeutic strategy targeting $KRAS^{G12D}$-driven circRNA biogenesis might achieved satisfied efficiency in the intervention of LN metastatic $KRAS^{G12D}$ PDAC.

We established a KPC mouse model to evaluate the therapeutic efficiency of circARFGEF2 in $KRAS^{G12D}$ PDAC LN metastasis. In KPC models, increasing circARFGEF2 expression markedly accelerated tumor growth, whereas inhibiting JAK2-STAT3 reversed this effect. In addition, blocking JAK2-STAT3 obviously impeded the promotion of circARFGEF2 in the lymphangiogenesis of primary PDAC tumors in the KPC model. Overall, our results provided sufficient support for the preclinical treatment effect of circARFGEF2 in $KRAS^{G12D}$ PDAC, indicating that circARFGEF2 is a potential therapeutic target in $KRAS^{G12D}$ PDAC.

In summary, we proposed a novel mechanism of $KRAS^{G12D}$ mutation-driven circARFGEF2 biogenesis via QKI-5-dependent splicing that mediated the miR-1205–JAK2–STAT3 axis to trigger PDAC LN metastasis. Inhibiting circARFGEF2 expression or the JAK2–STAT3 pathway significantly impeded tumor growth in the KPC model. These findings enabled new understanding of the regulatory mechanism in PDAC LN metastasis, suggesting that circARFGEF2 is a potential therapeutic target in $KRAS^{G12D}$ PDAC.

Authors' Disclosures

No author disclosures were reported.

Authors' Contributions

Y. Kong: Writing–original draft. **Y. Luo:** Investigation, methodology. **S. Zheng:** Data curation, validation. **J. Yang:** Project administration, writing–review and editing. **D. Zhang:** Data curation, formal analysis. **Y. Zhao:** Supervision, visualization. **H. Zheng:** Validation, project administration. **M. An:** Resources, software. **Y. Lin:** Validation, investigation, methodology. **L. Ai:** Software, formal analysis, methodology. **X. Diao:** Supervision, methodology. **Q. Lin:** Data curation, validation. **C. Chen:** Writing–original draft, project administration. **R. Chen:** Conceptualization, funding acquisition.

Acknowledgments

This study was funded by National Key Research and Development Program of China (grant no. 2022YFA1305500); the National Key Research and Development Program of China (grant no. 2018YFA0902803); National Natural Science Foundation of China (grant nos. 82072639, 82173272, 82103536, 82202276, 82103416, and 82203691); Guangdong Basic and Applied Basic Research Foundation (grant nos. 2023A1515011648, 2021B1515020091, 2022A1515012288, and 2021A1515010355); the Special Fund of "Dengfeng Plan" of Guangdong Provincial People's Hospital, China (grant nos. KJ012019509, DFJH2020027); the National Key Clinical Specialty Construction Project (grant no. 2022YW030009); China Postdoctoral Science Foundation (grant no. 2022T150147); and Guangdong Science and Technology Department (grant no. 2021A1515011089).

The publication costs of this article were defrayed in part by the payment of publication fees. Therefore, and solely to indicate this fact, this article is hereby marked "advertisement" in accordance with 18 USC section 1734.

Note

Supplementary data for this article are available at Cancer Research Online (http://cancerres.aacrjournals.org/).

Received December 23, 2022; revised April 5, 2023; accepted June 21, 2023; published first June 26, 2023.

References

1. Connor AA, Gallinger S. Pancreatic cancer evolution and heterogeneity: integrating omics and clinical data. Nat Rev Cancer 2022;22:131–42.
2. Park W, Chawla A, O'Reilly EM. Pancreatic cancer: a review. JAMA 2021;326:851–62.
3. Huang L, Guo Z, Wang F, Fu L. KRAS mutation: from undruggable to druggable in cancer. Signal Transduct Target Ther 2021;6:386.
4. Moore AR, Rosenberg SC, McCormick F, Malek S. RAS-targeted therapies: is the undruggable drugged? Nat Rev Drug Discov 2020;19:533–52.
5. O'Kane GM, Lowery MA. Moving the needle on precision medicine in pancreatic cancer. J Clin Oncol 2022;40:2693–705.
6. Pirlog R, Calin GA. KRAS mutations as essential promoters of lymphangiogenesis via extracellular vesicles in pancreatic cancer. J Clin Invest 2022;132:e161454.
7. Liu C-X, Chen L-L. Circular RNAs: characterization, cellular roles, and applications. Cell 2022;185:2016–34.
8. Li X, Yang L, Chen L-L. The biogenesis, functions, and challenges of circular RNAs. Mol Cell 2018;71:428–42.
9. Shi L, Magee P, Fassan M, Sahoo S, Leong HS, Lee D, et al. A KRAS-responsive long non-coding RNA controls microRNA processing. Nat Commun 2021;12:2038.
10. Panda AC, Grammatikakis I, Kim KM, De S, Martindale JL, Munk R, et al. Identification of senescence-associated circular RNAs (SAC-RNAs) reveals senescence suppressor CircPVT1. Nucleic Acids Res 2017;45:4021–35.
11. Chen J, Sun Y, Ou Z, Yeh S, Huang C-P, You B, et al. Androgen receptor-regulated circFNTA activates KRAS signaling to promote bladder cancer invasion. EMBO Rep 2020;21:e48467.
12. Nielsen AF, Bindereif A, Bozzoni I, Hanan M, Hansen TB, Irimia M, et al. Best practice standards for circular RNA research. Nat Methods 2022;19:1208–20.
13. Yang L, Wilusz JE, Chen L-L. Biogenesis and regulatory roles of circular RNAs. Annu Rev Cell Dev Biol 2022;38:263–89.
14. Xiao M-S, Ai Y, Wilusz JE. Biogenesis and functions of circular RNAs come into focus. Trends Cell Biol 2020;30:226–40.
15. Chen L-L. The expanding regulatory mechanisms and cellular functions of circular RNAs. Nat Rev Mol Cell Biol 2020;21:475–90.
16. Li J, Sun D, Pu W, Wang J, Peng Y. Circular RNAs in cancer: biogenesis, function, and clinical significance. Trends Cancer 2020;6:319–36.
17. Dou Y, Cha DJ, Franklin JL, Higginbotham JN, Jeppesen DK, Weaver AM, et al. Circular RNAs are down-regulated in KRAS mutant colon cancer cells and can be transferred to exosomes. Sci Rep 2016;6:37982.
18. Sharma M, Sharma S, Alawada A. Understanding the binding specificities of mRNA targets by the mammalian Quaking protein. Nucleic Acids Res 2019;47:10564–79.
19. Chen X, Liu Y, Xu C, Ba L, Liu Z, Li X, et al. QKI is a critical pre-mRNA alternative splicing regulator of cardiac myofibrillogenesis and contractile function. Nat Commun 2021;12:89.
20. Ren Y, Huo Y, Li W, He M, Liu S, Yang J, et al. A global screening identifies chromatin-enriched RNA-binding proteins and the transcriptional regulatory activity of QKI5 during monocytic differentiation. Genome Biol 2021;22:290.
21. Zhao L, Mandler MD, Yi H, Feng Y. Quaking I controls a unique cytoplasmic pathway that regulates alternative splicing of myelin-associated glycoprotein. Proc Natl Acad Sci U S A 2010;107:19061–6.
22. Conn SJ, Pillman KA, Toubia J, Conn VM, Salmanidis M, Phillips CA, et al. The RNA binding protein quaking regulates formation of circRNAs. Cell 2015;160:1125–34.
23. Bonnal SC, López-Oreja I, Valcárcel J. Roles and mechanisms of alternative splicing in cancer: implications for care. Nat Rev Clin Oncol 2020;17:457–74.
24. Sweha SR, Chung C, Natarajan SK, Panwalkar P, Pun M, Ghali A, et al. Epigenetically defined therapeutic targeting in H3.3G34R/V high-grade gliomas. Sci Transl Med 2023;13:eabf7860.
25. Kong LY, Wu AS, Doucette T, Wei J, Priebe W, Fuller GN, et al. Intratumoral mediated immunosuppression is prognostic in genetically engineered murine models of glioma and correlates to immunotherapeutic responses. Clin Cancer Res 2010;16:5722–33.
26. Kong LY, Abou-Ghazal MK, Wei J, Chakraborty A, Sun W, Qiao W, et al. A novel inhibitor of signal transducers and activators of transcription 3 activation is efficacious against established central nervous system melanoma and inhibits regulatory T cells. Clin Cancer Res 2008;14:5759–68.
27. Gupta SK, Garg A, Bär C, Chatterjee S, Foinquinos A, Milting H, et al. Quaking inhibits doxorubicin-mediated cardiotoxicity through regulation of cardiac circular RNA expression. Circ Res 2018;122:246–54.
28. Neumann DP, Goodall GJ, Gregory PA. The Quaking RNA-binding proteins as regulators of cell differentiation. Wiley Interdiscip Rev RNA 2022;13:e1724.
29. Hofmann MH, Gerlach D, Misale S, Petronczki M, Kraut N. Expanding the reach of precision oncology by drugging all KRAS mutants. Cancer Discov 2022;12:924–37.
30. Prenen H, Tejpar S, Van Cutsem E. New strategies for treatment of KRAS mutant metastatic colorectal cancer. Clin Cancer Res 2010;16:2921–6.
31. Karaman S, Detmar M. Mechanisms of lymphatic metastasis. J Clin Invest 2014;124:922–8.
32. Mumprecht V, Honer M, Vigl B, Proulx ST, Trachsel E, Kaspar M, et al. In vivo imaging of inflammation- and tumor-induced lymph node lymphangiogenesis by immuno-positron emission tomography. Cancer Res 2010;70:8842–51.
33. Kent SC, Chen Y, Bregoli L, Clemmings SM, Kenyon NS, Ricordi C, et al. Expanded T cells from pancreatic lymph nodes of type 1 diabetic subjects recognize an insulin epitope. Nature 2005;435:224–8.
34. Qadir J, Li F, Yang BB. Circular RNAs modulate Hippo-YAP signaling: functional mechanisms in cancer. Theranostics 2022;12:4269–87.
35. Danese S, Argollo M, Le Berre C, Peyrin-Biroulet L. JAK selectivity for inflammatory bowel disease treatment: does it clinically matter? Gut 2019;68:1893–9.
36. Yamaoka K, Saharinen P, Pesu M, Holt VET, Silvennoinen O, O'Shea JJ. The Janus kinases (Jaks). Genome Biol 2004;5:253.
37. Zhou C, Sun P, Xu Y, Chen Y, Huang Y, Hamblin MH, et al. Genetic deficiency of MicroRNA-15a/16–1 confers resistance to neuropathological damage and cognitive dysfunction in experimental vascular cognitive impairment and dementia. Adv Sci (Weinh) 2022;9:e2104986.
38. Kitajima S, Asahina H, Chen T, Guo S, Quiceno LG, Cavanaugh JD, et al. Overcoming resistance to dual innate immune and MEK inhibition downstream of KRAS. Cancer Cell 2018;34:439–52.
39. Han X, Mei Y, Mishra RK, Bi H, Jain AD, Schiltz GE, et al. Targeting pleckstrin-2/Akt signaling reduces proliferation in myeloproliferative neoplasm models. J Clin Invest 2023;133:e159638.
40. De Santis MC, Gozzelino L, Margaria JP, Costamagna A, Ratto E, Gulluni F, et al. Lysosomal lipid switch sensitises to nutrient deprivation and mTOR targeting in pancreatic cancer. Gut 2023;72:360–71.

41. Zhang Y, Chen X, Wang H, Gordon-Mitchell S, Sahu S, Bhagat TD, et al. Innate immune mediator, Interleukin-1 receptor accessory protein (IL1RAP), is expressed and pro-tumorigenic in pancreatic cancer. J Hematol Oncol 2022; 15:70.
42. De Kesel J, Fijalkowski I, Taylor J, Ntziachristos P. Splicing dysregulation in human hematologic malignancies: beyond splicing mutations. Trends Immunol 2022;43:674–86.
43. Buscail L, Bournet B, Cordelier P. Role of oncogenic KRAS in the diagnosis, prognosis and treatment of pancreatic cancer. Nat Rev Gastroenterol Hepatol 2020;17:153–68.
44. Sakers K, Liu Y, Llaci L, Lee SM, Vasek MJ, Rieger MA, et al. Loss of Quaking RNA binding protein disrupts the expression of genes associated with astrocyte maturation in mouse brain. Nat Commun 2021;12:1537.
45. Yamagishi R, Tsusaka T, Mitsunaga H, Maehata T, Hoshino S-i. The STAR protein QKI-7 recruits PAPD4 to regulate post-transcriptional polyadenylation of target mRNAs. Nucleic Acids Res 2016;44:2475–90.
46. Zhu Y-J, Zheng B, Luo G-J, Ma X-K, Lu X-Y, Lin X-M, et al. Circular RNAs negatively regulate cancer stem cells by physically binding FMRP against CCAR1 complex in hepatocellular carcinoma. Theranostics 2019;9: 3526–40.
47. Lu D, Chatterjee S, Xiao K, Riedel I, Huang C-K, Costa A, et al. A circular RNA derived from the insulin receptor locus protects against doxorubicin-induced cardiotoxicity. Eur Heart J 2022;43:4496–511.
48. Wu N, Qadir J, Yang BB. CircRNA perspective: new strategies for RNA therapy: (Trends in Molecular Medicine 28, 343–344; 2022). Trends Mol Med 2022;28: 530.